

TOPICAL REVIEW

Determination of the transfer function for optical surface topography measuring instruments—a review

Matthew R Foreman^{1,2}, Claudiu L Giusca², Jeremy M Coupland³,
Peter Török¹ and Richard K Leach²

¹ Blackett Laboratory, Department of Physics, Imperial College London, Prince Consort Road, London, SW7 2BZ, UK

² Engineering Measurement Division, National Physical Laboratory, Hampton Road, Teddington, Middlesex TW11 0LW, UK

³ Wolfson School of Mechanical and Manufacturing Engineering, University of Loughborough, Leicestershire, LE11 3TU, UK

E-mail: matthew.foreman@imperial.ac.uk and richard.leach@npl.co.uk

Received 2 November 2012, in final form 14 January 2013

Published 21 March 2013

Online at stacks.iop.org/MST/24/052001

Abstract

A significant number of areal surface topography measuring instruments, largely based on optical techniques, are commercially available. However, implementation of optical instrumentation into production is currently difficult due to the lack of understanding of the complex interaction between the light and the component surface. Studying the optical transfer function of the instrument can help address this issue. Here a review is given of techniques for the measurement of optical transfer functions. Starting from the basis of a spatially coherent, monochromatic confocal scanning imaging system, the theory of optical transfer functions in three-dimensional (3D) imaging is presented. Further generalizations are reviewed allowing the extension of the theory to the description of conventional and interferometric 3D imaging systems. Polychromatic transfer functions and surface topography measurements are also discussed. Following presentation of theoretical results, experimental methods to measure the optical transfer function of each class of system are presented, with a focus on suitable methods for the establishment of calibration standards in 3D imaging and surface topography measurements.

Keywords: areal surface topography, optical transfer function, optical instruments, point spread function, linear theory

(Some figures may appear in colour only in the online journal)

Abbreviations

NA numerical aperture
PSF point spread function
LSF line spread function
ESF edge spread function
OTF optical transfer function
CTF coherent transfer function

MTF modulation transfer function
PTF phase transfer function
WOTF weak object transfer function
DHM digital holographic microscope
CPM coherence probe microscope
SPM scanning probe microscope
OCT optical coherence tomography
CCM confocal chromatic microscopy

CSI	coherence scanning interferometry
DSI	dispersive scanning interferometry
TCC	transmission cross-coefficient

1. Introduction

The performance and functional properties of a large number of engineered surfaces and parts can depend strongly on their topographical and textural characteristics. For example, surface deviations in ground optical lenses can give rise to optical aberrations degrading imaging quality, whilst roughness in engine parts can lead to increased wear and shorter component lifetimes. Conversely, increased wear can also improve the functional performance of a surface. Accordingly, the determination of surface properties has long been an important problem since this can play a crucial role in controlling manufacturing procedures and allowing quality control of components such as MEMS wafers, industrial coatings, optical lenses and machined parts. Furthermore, in many situations information gained from surface topography data permits development of new product specifications with enhanced functionality.

Historically, a number of complementary techniques have been employed to perform surface topography measurements, namely stylus- and optical-probe-based instruments [1, 2]. Mechanical-stylus-based instruments were initially exclusively used to measure height variations with high resolution, whilst optical methods were oriented towards the measurement of a transverse structure. However, as these techniques have developed so their three-dimensional (3D) and areal capabilities have converged in the so-called horns of metrology [3]. Greater demands are, however, being made of surface metrology particularly at nanometre scales, where high resolution and rapid data acquisition are sought. Optical techniques, such as conventional Michelson and Twyman–Green interferometry [4], Schmaltz light sectioning microscopy [5], Tolansky multiple beam interferometry [6], fringes of equal chromatic order interferometry [7], Linnik microminterferometry [8], Mirau interferometry [9], phase shifting interferometry [10], coherence scanning/white light interferometry [11, 12] and confocal microscopy [13], have the potential to satisfy these needs.

An important issue that must be addressed to bring surface topography into compliance with manufacturing quality systems is the measurement traceability of the instruments. Whilst there is a traceability infrastructure for stylus instruments operating in a profile mode [4], there is not yet a satisfactory infrastructure for areal surface topography measuring instruments. To fill the traceability chain from the definition of the metre to an areal measurement in industry, a number of steps are required (see figure 1). Firstly, primary instrumentation that can measure areal surface topography is needed. A number of national measurement institutes (including the National Physical Laboratory (NPL) in the UK) have developed stylus instruments with displacement measuring laser interferometers that can determine the position of the stylus tip [14, 15]. Knowledge of the laser source wavelength in the interferometers assures traceability to the

definition of the metre. Secondly, transfer artefacts are needed that can be calibrated via the primary instrumentation (either directly or indirectly) and used in turn to calibrate instruments in industry.

NPL has been working towards a traceability infrastructure for areal measurement for a decade, for both stylus based and optical systems. Significant effort has, for example, been made towards the production of low cost, calibrated artefacts and good practice guides for stylus instruments, phase stepping and coherence scanning interferometers and scanning confocal microscopes. Artefacts and guides for focus variation microscopy are also expected shortly. The general philosophy behind the calibration schemes developed can, however, be extended to most commercial instruments. A stylus-based primary instrument has also been developed and methods for calculating uncertainties using this instrument, based on a Monte Carlo approach, devised [16]. Calibration protocols and evaluation techniques have also been developed at NPL, such as those detailed in [17–19], using bespoke primary instrumentation [14]. These protocols, however, address only the calibration of the scales of an areal surface topography measuring instrument. The calibration consists of measuring the noise and flatness of the instrument, amplification coefficients, linearity and squareness of the scales, which although common to all instrument types, do not give a complete system characterization. These parameters, for example, do not describe the response of the system to sloped surfaces. Similarly the Physikalisch-Technische Bundesanstalt (PTB) provide artefacts for the calibration of vertical and lateral measurements of contact stylus instruments. PTB also provide an online review of calibration artefacts used for dimensional measurement of microstructures [20] and those used for the calibration of scanning probe microscopes (SPMs) [21]. The calibration artefact of Ritter *et al* also stands as a notable compliment to those available for calibration of SPMs. A number of artefacts are also available from the National Institute of Standards and Technology (NIST) and other manufacturers and researchers [22–25]. Such calibration artefacts, however, are either intended for the calibration of restricted system parameters, e.g. lateral resolution, or for determining the so-called instrument transfer function. Whilst the former inherently does not provide a complete characterization of a measurement system, the latter provides a description of all stages in the measurement system including (potentially nonlinear) digital image processing stages as a whole. As such the instrument transfer function provides limited insight into the origin of factors degrading and limiting image quality. Measurement of the optical transfer function (OTF) of the system provides complete information as to the imaging properties of an instrument, however, and is for this reason being actively pursued [26, 27]. A standard measurement technique has nevertheless still to be agreed. This paper focuses on reviewing work done to date on measuring the OTF as a basis from which to build such a standard (see also [28–31]).

In this context, section 2 covers the basics of linear optical theory in which the OTFs of common 3D imaging architectures are defined and discussed. Much of the relevant theory exists

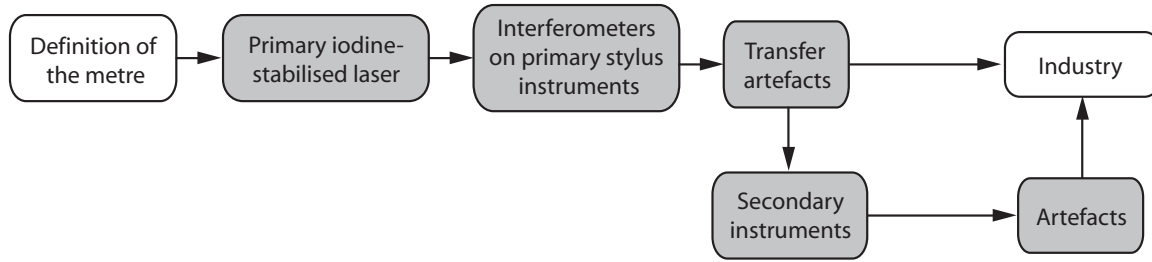


Figure 1. Flow diagram of the steps required for areal traceability to the metre. Note that in practice there would be another stabilized laser between the primary laser and the interferometers.

in the literature and so only the fundamentals are reproduced here; however, appropriate references are given throughout for the interested reader. Section 3 proceeds to discuss techniques reported in the literature of how OTFs can, and have been measured in practice. A concluding discussion and viewpoint is given in section 4.

2. Three-dimensional linear theory in optical metrology

Any measurement system can be regarded as a mathematical mapping from a set of input functions to an associated set of output functions. The system output can thus be represented as $v(\mathbf{r}) = M[u(\mathbf{r}')]$, where \mathbf{r} and \mathbf{r}' are coordinates in output and input space, respectively, and $M[\cdot \cdot \cdot]$ represents the mapping from $u(\mathbf{r}')$ to $v(\mathbf{r})$.

A common approximation in many systems is to assume that the function $M[\cdot \cdot \cdot]$ is linear, such that the principle of superposition holds. Within the context of optical metrology, this approximation equates to assuming multiple scattering is negligible and that the Born approximation holds (see section 2.1). Accordingly, if the input function is represented as a superposition of point-like elements, then the system output is given by

$$v(\mathbf{r}) = \int_{V'} u(\mathbf{s})M[\delta(\mathbf{r}' - \mathbf{s})] d\mathbf{s} = \int_{V'} u(\mathbf{s})h(\mathbf{r}, \mathbf{s}) d\mathbf{s}, \quad (1)$$

where \mathbf{s} is a dummy variable and V' is the domain of the input function. The function $h(\mathbf{r}, \mathbf{s})$ is known as the impulse response of the measurement system or, in the case of optical instruments, as the point spread function (PSF). Physically, the PSF describes the output from a single elementary input or scattering source. Further assuming the measurement system to be spatially shift-invariant implies the PSF is dependent only on the difference of coordinates such that $h(\mathbf{r}, \mathbf{s}) = h(\mathbf{r} - \mathbf{s})$. It should be noted that there may exist an implicit scaling in the coordinates (e.g. as may be associated with the magnification of an imaging setup). Under these assumptions, equation (1) can then be expressed as a 3D convolution, namely

$$v(\mathbf{r}) = h(\mathbf{r}) \otimes_3 u(\mathbf{r}) = \int_{\infty} u(\mathbf{s})h(\mathbf{r} - \mathbf{s}) d\mathbf{s}, \quad (2)$$

where the integration limits are over all space, such that the function $u(\mathbf{s})$ is now assumed to adopt a zero value outside the domain V' .

Whilst it is insightful and intuitive to analyse a measurement system in terms of its response to point-like inputs, an alternative choice of an elementary input function commonly considered is that of a sinusoidally varying function. This analysis ultimately dates back to the work of Fourier, but was first considered in optical imaging by Duffieux [32] in 1946, following the sine-wave tests of Selwyn [33]. In this vein, it is necessary to move from the spatial domain (described by \mathbf{r} and \mathbf{r}') to a spatial frequency domain, whereby the 3D spectrum of the source and output distribution can be defined via a 3D inverse Fourier transform, namely

$$\tilde{u}(\mathbf{m}) = \int_{\infty} u(\mathbf{r}') e^{-2\pi i \mathbf{m} \cdot \mathbf{r}'} d\mathbf{r}' \quad (3)$$

(and similarly for $\tilde{v}(\mathbf{m})$), where $\mathbf{m} = (m, n, q)$ is a triplet of spatial frequencies. It should be noted that the $\tilde{f}(\mathbf{m})$ notation will be used throughout this text to signify the Fourier representation of a function $f(\mathbf{r})$ and that all limits on integrals will be assumed to be over an infinite domain. In the Fourier domain, the convolution of equation (2) becomes the mathematically simpler product $\tilde{v}(\mathbf{m}) = \tilde{h}(\mathbf{m})\tilde{u}(\mathbf{m})$, where $\tilde{h}(\mathbf{m})$ is the so-called OTF, given by the inverse Fourier transform of the PSF.

The function $\tilde{h}(\mathbf{m})$ warrants further discussion, particularly in the context of optical metrology. Fundamental to any optical metrology setup is a 3D imaging setup, with object parameters, such as surface height or roughness, derived from a 3D image via appropriate data processing. An interferometric detection architecture is also commonly used. In optical imaging systems, however, the light source may be coherent (e.g. laser illumination), incoherent (e.g. tungsten lamp) or even partially coherent. Moreover, the scattering and/or detection process may also fall into any of these same three categories (e.g. a fibre-optic scanning confocal reflection microscope, fluorescence microscope or conventional microscope [34–36]). Importantly, these different possibilities necessitate different system models, particularly with regards to which optical variable the system is linear in. For coherent systems, the OTF is more specifically referred to as the coherent transfer function (CTF) which describes both the attenuation and phase shift introduced in the image of a sinusoidal field pattern (or scattering potential if the Born approximation is satisfied, cf section 2.1), i.e. the system is ‘linear in complex field’. Importantly, if the Born approximation is also satisfied, then the system can also be said to be ‘linear in scattering potential’. The modulus of the CTF

is known as the modulation transfer function (MTF), whilst the argument is termed the phase transfer function (PTF) [37]. An OTF, MTF and PTF can be defined analogously for an incoherent case; however, in this case the system is 'linear in intensity', or, if the Born approximation is satisfied, the system is also 'linear in the square of the scattering potential'. Partially coherent systems are inherently more complicated, with image formation no longer describable using an OTF. Instead, the so-called transmission cross-coefficient (TCC) [36, 38] must be defined which describes the attenuation and relative phase shift upon imaging *pairs* of spatial frequencies (of the underlying time instantaneous field). Definition of the so-called weak object transfer function (WOTF) is sometimes possible in a partially coherent system if scattering from the object can be considered weak [34]; however, this will not be discussed further here for the sake of brevity.

Studies of OTFs were perhaps first initiated by Dändliker and Weiss [39], and by Wolf [40], who discussed the reconstruction of the 3D refractive index distribution of a semi-transparent scattering object from scattered waves and holographic measurements, respectively. Both treatments, however, described 3D imaging theory in a coherent system only. The first treatment of incoherent systems was presented by Frieden who developed a 3D transfer function theory [41], by extending the 2D transfer function originally proposed by Duffieux [32]. A partially coherent treatment of image formation was first presented by Hopkins in his seminal work [42], albeit in a 2D manner, with the 3D treatment given by Striebl [36]. Striebl's work was, however, an approximate treatment in which bilinear terms were neglected. Image formation in confocal microscopes has been shown to fall into a class of imaging systems not considered in Hopkin's or Striebl's original work [43]. As such, Sheppard and Mao extended their work to include the bilinear terms and hence provide a more accurate description of imaging in both conventional and confocal arrangements [38]. Formally, 3D imaging can be considered by an introduction of defocused pupil functions into existing 2D treatments [44, 45]. As such it is worthwhile to mention the work of Sheppard and Wilson on 2D image formation in scanning microscopy [46–49]. However, an alternative is to use a full 3D CTF treatment, such as that presented in [34, 35, 50–55]. The derivations presented in these works are, however, for ideal systems. Deviations from such ideal circumstances and their effect on the OTF of imaging systems have been considered in [56, 57], for example.

For high NA (i.e. $NA \gtrsim 0.5$) systems, departures from the more common paraxial theory presented in the above-cited articles arise due to three main effects. The first of these is that waves propagating in the system can do so at large angles to the optical axis, such that the inherent small angle expansions are no longer valid. Secondly, polarization properties of light become important due to the introduction of a non-negligible longitudinal component in object space. Finally, in moving away from a low NA system the pupil function of a lens can also no longer be specified in the pupil plane of the lens. Instead, the pupil function must be specified over the surface of the Gaussian reference sphere [58] located in the exit pupil centred

on the geometric focus of the lens (cf equation (9)), introducing an additional apodisation effect. In this vein, Sheppard *et al* [59, 60] have approached the generalization of the OTF to high NA systems avoiding the paraxial approximation; however, vectorial effects were not included. The apodisation effect has also been considered [61]. Vectorial transfer functions have been considered within a paraxial regime by Urbańczyk [62–64], albeit this work considered only 2D image formation. A fuller 3D vectorial theory has however been proposed by Arnison and Sheppard [65], and Sheppard and Larkin [66] which also relaxes the paraxial approximation. These ideas have, however, not received significant attention in the literature, due to the underlying mathematical complexity.

A final issue worthy of note is the assumption of shift invariance in high NA imaging systems. Particularly, the amplitude PSF is, in general, not shift invariant such that this assumption is not valid. If however 3D object scanning is used, it is evident that the imaging properties of the optical system are unchanged with object position, such that 3D shift invariance can safely be assumed. Full 3D object scanning is however not required if the lens satisfies the sine condition, such that the apodisation function takes the form $a(\theta) = \sqrt{\cos \theta}$, which produces transverse shift invariance. Full 3D shift invariance can hence be maintained if only axial object scanning is used [31].

Given the array of different imaging configurations, it seems a somewhat arduous task to analyse all possible imaging configurations. Equivalencies between confocal and conventional arrangements and scanning microscopes of differing geometries have, however, been expounded [31, 43] reducing the number of distinct geometries that need be considered. This equivalence originates from Helmholtz's principle of reversibility. As such, in this document it is only necessary to describe a scanning confocal microscope with either a point, or infinite, intensity sensitive detector for both coherent and incoherent illumination as is done in sections 2.2 and 2.3, respectively. A description of partially coherent systems will naturally emerge in these discussions. Interferometric arrangements will also be considered and the OTF for the interference image is presented in section 2.4. Polarization effects will not be considered, however, due to the extra level of complexity required to fully account for such features and the additional difficulties associated with measuring vectorial transfer functions. Measurements of such vectorial transfer functions are also difficult to find in the literature. Moreover, only reflection geometries are to be considered as this is the usual operational setup in optical metrology. The equivalencies of each system geometry will be indicated where appropriate. Before proceeding to describe the OTF for these geometries, it is first necessary to consider the nature of the process by which an illuminating field is scattered from a sample of interest, as discussed in the following section.

2.1. Scattering theory and the Born approximation

Since engineering surfaces are not self-luminous, it is necessary to illuminate them with a known field and measure the light subsequently scattered from the object. The standard

starting point for a derivation of the scattered field (see e.g. [58]) is the scalar wave equation,

$$\nabla^2 E(\mathbf{r}) + k^2 n^2(\mathbf{r}) E(\mathbf{r}) = 0, \quad (4)$$

where $E(\mathbf{r})$ is the complex scalar field at position \mathbf{r} in a medium of refractive index $n(\mathbf{r})$, assumed to be monochromatic with time dependence $\exp(-i\omega t)$ and $k = \omega/c = 2\pi/\lambda$ is the associated wavenumber in vacuum. When a field is incident on an inhomogeneity in the refractive index, a scattered field results. As such the resulting field is a superposition of the original incident field and the scattered field, i.e. $E = E_r + E_s$. Hence,

$$\nabla^2 (E_r(\mathbf{r}) + E_s(\mathbf{r})) + k^2 n^2(\mathbf{r}) (E_r(\mathbf{r}) + E_s(\mathbf{r})) = 0. \quad (5)$$

Noting that E_r is the illumination field that must satisfy the scalar wave equation in the absence of the scattering object, i.e. $\nabla^2 E_r(\mathbf{r}) + k^2 E_r(\mathbf{r}) = 0$ yields

$$(\nabla^2 + k^2) E_s(\mathbf{r}) = t(\mathbf{r}) (E_r(\mathbf{r}) + E_s(\mathbf{r})), \quad (6)$$

where $t(\mathbf{r}) = k^2 [n^2(\mathbf{r}) - 1]$ is known as the scattering potential. Equation (6) takes the form of a free-space scalar wave equation with the source term (or scattering function) $U(\mathbf{r}) = t(\mathbf{r}) (E_r(\mathbf{r}) + E_s(\mathbf{r}))$. Accordingly, equation (6) can thus be solved using the well-known free-space Green's function $G(\mathbf{r}) = \exp(ik|\mathbf{r}|)/4\pi|\mathbf{r}|$ [67] to give $E_s(\mathbf{r}) = G(\mathbf{r}) \otimes_3 U(\mathbf{r})$.

In linear optical scattering, a further approximation is generally adopted to permit tractable mathematical analysis. Specifically, the first Born approximation states that the source term $U(\mathbf{r}) = U_r(\mathbf{r}) + U_s(\mathbf{r})$ can be replaced by $U_r(\mathbf{r})$, that is to say that the object scatters weakly such that

$$U(\mathbf{r}) \approx t(\mathbf{r}) E_r(\mathbf{r}). \quad (7)$$

Neglecting effects arising from multiple scattering and depletion of the illumination beam is also implicit in making the Born approximation. Accordingly, the interaction with the object can be considered as reflection from a sample with complex reflection coefficient $t(\mathbf{r}) = k^2 [n^2(\mathbf{r}) - 1]$. Indeed, if the Born approximation is valid, then the output field of an imaging system can be said to be linearly related to the scattering potential or effective reflection coefficient, as per equation (7). Equally the scattered intensity from an object is linearly related to $|t(\mathbf{r})|^2$, i.e. the effective reflectivity. This assumption will be seen to enable derivation of the OTF in a number of complex optical systems. A discussion on the validity of adopting the Born approximation can be found in [68]. Finally, it should be noted that throughout this section no mention of any optics that may modify the form of the field incident onto the scattering object has been made, since such effects can be included in the PSF (and hence also the OTF) of an optical system. An example of this will be seen in the following section.

2.2. Confocal and conventional coherent imaging systems

In this section, the pertinent theory from the above literature is distilled into a derivation of the CTF for imaging in

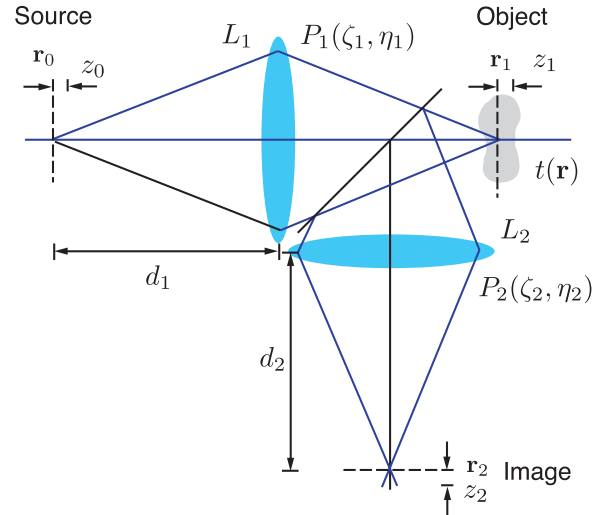


Figure 2. Schematic of the optical setup and coordinate geometry of a reflection type microscope, comprising two lenses L_1 and L_2 with associated pupil functions $P_1(\zeta_1, \eta_1)$ and $P_2(\zeta_2, \eta_2)$, respectively. A weakly scattering object is assumed present with scattering properties described by $t(\mathbf{r})$.

both confocal and conventional coherent imaging systems. Following from the equivalence theorem presented in [31, 43], the CTF will be derived by considering a confocal scanning system with a point detector and infinite incoherent detector, respectively.

Consider then the setup shown in figure 2, which depicts the basic arrangement of a confocal imaging system operating in a reflection mode. A point source is imaged onto the object of interest by means of an objective lens L_1 . The light back scattered is then imaged onto a detector by means of the collector lens L_2 . It should be noted that naming conventions for these lenses depend on the exact imaging geometry [49]. In practical systems, a single lens is used to perform the role of both objective and collector.

The 3D PSF of each lens is given by [31]

$$h_j(\mathbf{r}) = \int \tilde{h}_j(\mathbf{m}) e^{2\pi i \mathbf{m} \cdot \mathbf{r}} d\mathbf{m}, \quad (8)$$

where

$$\tilde{h}_j(\mathbf{m}) = \frac{P_j(m, n)}{q} \delta(q - \sqrt{1/\lambda^2 - m^2 - n^2}). \quad (9)$$

Here, $P_j(m, n)$ is the 2D pupil function of lens L_j . The Dirac delta function demonstrates that the pupil function of a high NA lens is defined over a spherical cap in the Fourier domain. Integration over q can be analytically performed to give

$$h_j(\mathbf{r}) = \iint \frac{P_j(m, n, z)}{\sqrt{1/\lambda^2 - m^2 - n^2}} \exp[2\pi i(mx + ny)] dm dn, \quad (10)$$

where

$$P_j(m, n, z) = P_j(m, n) \exp[2\pi i z \sqrt{1/\lambda^2 - m^2 - n^2}] \quad (11)$$

is known as the defocused pupil function. Henceforth assuming, for simplicity, that the point source is placed on axis at $\mathbf{r}_0 = \mathbf{0}$ implies the field incident on the object plane is

given by $E_r(\mathbf{r}_1) = h_1(\mathbf{r}_1)$. From equation (7), the scattering function (assuming the object has been scanned to a position \mathbf{r}_s) becomes

$$U(\mathbf{r}_1, \mathbf{r}_s) \approx t(\mathbf{r}_s - \mathbf{r}_1)h_1(\mathbf{r}_1). \quad (12)$$

Following linear imaging theory, the field at a position \mathbf{r}_2 in detector space is given by the convolution of the PSF of the collector lens with the source function $U(\mathbf{r}_1, \mathbf{r}_s)$. Treating this field as a function of the object scan position gives

$$E_d(\mathbf{r}_s, \mathbf{r}_2) = \int h_1(\mathbf{r}_1)h_2(\mathbf{r}_1 + \mathbb{M}_2\mathbf{r}_2)t(\mathbf{r}_s - \mathbf{r}_1) d\mathbf{r}_1 \quad (13)$$

where, following [31], \mathbb{M}_2 is a diagonal 3×3 matrix with diagonal elements describing the transverse and axial magnifications. Equation (13) demonstrates the linear relationship between the field incident onto the detector and the scattering potential in a coherent system. An effective PSF can hence be defined for the system as [50]

$$h_{\text{eff}}(\mathbf{r}_1, \mathbf{r}_2) = h_1(\mathbf{r}_1)h_2(\mathbf{r}_1 + \mathbb{M}_2\mathbf{r}_2) \quad (14)$$

along with the corresponding CTF $\tilde{h}_{\text{eff}}(\mathbf{m}, \mathbf{r}_2)$. For a general finite sized detector described by the response function $D(\mathbf{r}_2)$, the intensity recorded for each scan position is given by

$$I_d(\mathbf{r}_s) = \int |E_d(\mathbf{r}_s, \mathbf{r}_2)|^2 D(\mathbf{r}_2) d\mathbf{r}_2. \quad (15)$$

Through its dependence on the 3D position vector \mathbf{r}_2 , the response function $D(\mathbf{r}_2)$ allows for a general detection configuration, such as a tilted CCD, tomographic projections etc. In what follows however restriction will be made to ideal confocal (denoted by the subscript cf) and conventional (cv) imaging systems which employ a point detector at \mathbf{r}_d or an infinite planar detector at z_d , respectively, such that $D_{\text{cf}}(\mathbf{r}_2) = \delta(\mathbf{r}_2 - \mathbf{r}_d)$ and $D_{\text{cv}}(\mathbf{r}_2) = \delta(z_2 - z_d)$. Using equations (13)–(15) and their Fourier domain equivalents yields

$$I_d(\mathbf{r}_s) = \iint \tilde{H}(\mathbf{m}, \mathbf{m}') \tilde{t}(\mathbf{m}) \tilde{t}^*(\mathbf{m}') \times \exp[2\pi i \mathbf{r}_s \cdot (\mathbf{m} - \mathbf{m}')] d\mathbf{m} d\mathbf{m}', \quad (16)$$

where

$$\tilde{H}(\mathbf{m}, \mathbf{m}') = \int \tilde{h}_{\text{eff}}(\mathbf{m}, \mathbf{r}_2) \tilde{h}_{\text{eff}}^*(\mathbf{m}', \mathbf{r}_2) D(\mathbf{r}_2) d\mathbf{r}_2 \quad (17)$$

is the TCC introduced above. It can be seen from equation (16) that, in this general case, the linear dependence of the system on the scattering potential is lost due to the product $\tilde{t}(\mathbf{m}) \tilde{t}^*(\mathbf{m}')$. For an ideal confocal system, the sifting property of the Dirac delta function in the response function immediately gives the detected confocal signal as $|E_d(\mathbf{r}_s, \mathbf{r}_d)|^2$, thus implying the confocal CTF is given by $\tilde{h}_{\text{cf}}(\mathbf{m}, \mathbf{r}_d) = \tilde{h}_{\text{eff}}(\mathbf{m}, \mathbf{r}_d)$. For the simple case of an on-axis detector ($\mathbf{r}_d = \mathbf{0}$), the confocal PSF reduces to $h_{\text{cf}}(\mathbf{r}_1, \mathbf{0}) = h_1(\mathbf{r}_1)h_2(\mathbf{r}_1)$ and the CTF becomes

$$\tilde{h}_{\text{cf}}(\mathbf{m}, \mathbf{0}) = \left\{ \frac{P_1(m, n)}{q} \delta(q - \sqrt{1/\lambda^2 - m^2 - n^2}) \right\} \otimes_3 \left\{ \frac{P_2(m, n)}{q} \delta(q - \sqrt{1/\lambda^2 - m^2 - n^2}) \right\}. \quad (18)$$

Furthermore, the confocal TCC becomes separable in \mathbf{m} and \mathbf{m}' such that $\tilde{H}_{\text{cf}}(\mathbf{m}, \mathbf{m}') = \tilde{h}_{\text{cf}}(\mathbf{m}, \mathbf{0}) \tilde{h}_{\text{cf}}^*(\mathbf{m}', \mathbf{0})$.

Image formation in a conventional imaging system however does not give a separable TCC. Instead the TCC in this case is given by

$$\tilde{H}_{\text{cv}}(\mathbf{m}, \mathbf{m}') = \int \tilde{h}_1(\mathbf{m} - \mathbf{m}'') \tilde{h}_1^*(\mathbf{m}' - \mathbf{m}'') |\tilde{h}_2(\mathbf{m}'')|^2 d\mathbf{m}'' \quad (19)$$

Note the equivalence between a confocal setup with an infinite detector and a conventional imaging system dictates that the pupil function for the condenser lens in the conventional system is the same as that for the collector in the confocal system and the objective lens in each system is identical [38]. Accordingly, in equation (19), the P_1 and P_2 terms, implicit in the \tilde{h}_1 and \tilde{h}_2 factors, refer to the pupil functions of the objective and condenser lens, respectively. It is noted that phase aberrations in the condenser lens are irrelevant with regards to determining the TCC, such that if it is assumed that the condenser is perfectly transmitting, the TCC reduces to

$$\tilde{H}_{\text{cv}}(\mathbf{m}, \mathbf{m}') = \int \tilde{h}_1(\mathbf{m} - \mathbf{m}'') \tilde{h}_1^*(\mathbf{m}' - \mathbf{m}'') d\mathbf{m}'' \quad (20)$$

For later reference, the image of a point object in a coherent system is briefly considered. For a point object $t(\mathbf{r}) = \delta(\mathbf{r} - \mathbf{r}_o)$, the measured intensity derived from the square of equation (13) reduces to

$$I_d(\mathbf{r}_s, \mathbf{r}_o) = |h_1(\mathbf{r}_s - \mathbf{r}_o)|^2 \int |h_2(\mathbf{r}_s - \mathbf{r}_o + \mathbb{M}_2\mathbf{r}_2)|^2 D(\mathbf{r}_2) d\mathbf{r}_2 \quad (21)$$

which is known as the intensity PSF. For a point detector (such as in the ideal confocal case), the intensity PSF is given by

$$H_{\text{cf}}(\mathbf{r}_s, \mathbf{r}_o) = |h_1(\mathbf{r}_s - \mathbf{r}_o)|^2 |h_2(\mathbf{r}_s - \mathbf{r}_o + \mathbb{M}_2\mathbf{r}_d)|^2 \quad (22)$$

as would be expected by squaring the amplitude PSF of equation (14). However, for an infinite detector, as is equivalent to a conventional imaging system, equation (21) reduces to

$$H_{\text{cv}}(\mathbf{r}_s, \mathbf{r}_o) = |h_1(\mathbf{r}_s - \mathbf{r}_o)|^2 \quad (23)$$

since convolution with an infinite uniform function has no functional dependence and can be dropped. A common misconception is that whilst equations (22) and (23) express the image of a point object, equations (13) and (15) do not represent the sum of the intensity scattered from each point on an object for a coherent system. This issue will be further discussed in the following section.

2.3. Confocal and conventional incoherent imaging systems

Whilst the preceding section considered image formation in coherent optical systems in which the imaging process acts as a linear filter in field amplitude, incoherent imaging acts as a linear filter in intensity. Incoherent imaging models must be used if, for example, an extended incoherent source is used, or if phase coherence from the illumination field is lost during interaction with the sample, such as in a fluorescence microscope. In optical metrology, the use of an extended

incoherent illumination is, by far, the more relevant of these two scenarios. That said, a one-photon fluorescence model will be used here [34] and the equivalences detailed in [43] again invoked, such that the imaging geometries adopted thus far (i.e. point source) can be maintained and the mathematical framework does not require significant modification.

To begin equation (7) is revisited. Given that phase coherence is assumed to be lost, scattering must be described as a spatially incoherent process whereby $I(\mathbf{r}) = T(\mathbf{r})I_r(\mathbf{r})$, where $T(\mathbf{r}) = |t(\mathbf{r})|^2$ and $I_r(\mathbf{r})$ is the illuminating intensity. It follows that $I(\mathbf{r}_1) = |h_1(\mathbf{r}_1)|^2 T(\mathbf{r}_1)$ and for an incoherent imaging process the intensity in detector space, for an object scanned to \mathbf{r}_s , is given by

$$I_d(\mathbf{r}_s, \mathbf{r}_2) = \int |h_1(\mathbf{r}_1)|^2 |h_2(\mathbf{r}_1 + \mathbb{M}_2 \mathbf{r}_2)|^2 T(\mathbf{r}_s - \mathbf{r}_1) d\mathbf{r}_1 \quad (24)$$

in a similar fashion to above. In contrast to equation (13), equation (24) shows the linear relationship between detected intensity and the modulus squared of the scattering potential in an incoherent system. Following earlier discussions the intensity recorded by a finite-sized detector is hence

$$I_d(\mathbf{r}_s) = \int H(\mathbf{r}_1) T(\mathbf{r}_s - \mathbf{r}_1) d\mathbf{r}_1, \quad (25)$$

where now

$$H(\mathbf{r}_1) = \int |h_1(\mathbf{r}_1)|^2 |h_2(\mathbf{r}_1 + \mathbb{M}_2 \mathbf{r}_2)|^2 D(\mathbf{r}_2) d\mathbf{r}_2 \quad (26)$$

is the intensity PSF for a point object at \mathbf{r}_1 . Restricting to the ideal confocal (point detector) and conventional (infinite detector) cases gives

$$H_{cf}(\mathbf{r}_s, \mathbf{r}_o) = |h_1(\mathbf{r}_s - \mathbf{r}_o)|^2 |h_2(\mathbf{r}_s - \mathbf{r}_o + \mathbb{M}_2 \mathbf{r}_d)|^2 \quad (27)$$

and

$$H_{cv}(\mathbf{r}_s, \mathbf{r}_o) = |h_1(\mathbf{r}_s - \mathbf{r}_o)|^2, \quad (28)$$

respectively. Comparing equations (27) and (28) to equations (22) and (23) it is seen that the intensity PSFs for the coherent and incoherent systems are identical in form. That said the resulting images differ by virtue of the difference between equations (13) and (25).

As highlighted by Gu in [34], the equivalence of the intensity PSFs in coherent and incoherent imaging systems highlights the inadequacy of the PSF description of imaging systems. Instead an OTF description is deemed more fundamental since differences can be seen here. Indeed, following [41], the 3D OTF in an incoherent system is defined as the 3D inverse Fourier transform of the intensity PSF, namely

$$\tilde{H}(\mathbf{m}) = \int H(\mathbf{r}_1) \exp[-2\pi i \mathbf{r}_1 \cdot \mathbf{m}] d\mathbf{r}_1. \quad (29)$$

Defining the object and image spectra (denoted $\tilde{T}(\mathbf{m})$ and $\tilde{I}(\mathbf{m})$ respectively) in a similar fashion, the convolution integral expressed in equation (25) can be written in the Fourier domain as

$$\tilde{I}(\mathbf{m}) = \tilde{H}(\mathbf{m}) \tilde{T}(\mathbf{m}). \quad (30)$$

In relation to the definition of the OTF given in equation (29), it is important to note that whilst for the confocal case the intensity PSF is given by the square of the amplitude PSF, the OTF is not given by the square of the CTF. The incoherent OTF is in fact related to the CTF of the analogous system via the convolution integral $\tilde{H}_{eff}(\mathbf{m}) = \tilde{H}_{eff-1}(\mathbf{m}) \otimes_3 \tilde{H}_{eff-2}(\mathbf{m})$, where

$$\begin{aligned} \tilde{H}_{eff-n}(\mathbf{m}) &= \int |h_n(\mathbf{r})|^2 \exp[-2\pi i \mathbf{r} \cdot \mathbf{m}] d\mathbf{r} \\ &= \tilde{h}_n^*(\mathbf{m}) \star \tilde{h}_n(\mathbf{m}'), \end{aligned} \quad (31)$$

and \star denotes a 3D correlation. Likewise, for a conventional imaging arrangement the incoherent OTF is given by the autocorrelation of the amplitude PSF of the objective lens, i.e. $\tilde{H}_{cv}(\mathbf{m}) = \tilde{h}_1^*(\mathbf{m}) \star \tilde{h}_1(\mathbf{m})$. This observation will be required in section 3.

2.4. Confocal and conventional interferometric setups

Interferometric microscopes can be found in numerous configurations, such as the Linnik, Mirau, Michelson, Fizeau, Mach–Zehnder or confocal interferometers [69]. Each has its own advantages and disadvantages [70]; however, in all geometries the field scattered from the object is combined with that of a reference beam. Imaging in an interference microscope has previously been considered in, for example, [47, 71–73]. The setup considered in [47], for example, is based upon a Mach–Zehnder configuration. Moreover, it should be noted that a digital holographic microscope (DHM) is based upon a Mach–Zehnder architecture, albeit without any lenses present in the reference arm [40]. As such the wavefront in the reference arm is less important in a DHM [74, 75]. Derivations for the CTF of a confocal interferometer and a fibre-optical confocal interferometer can be found in [34, 76].

In this section, both confocal and conventional interferometric microscopy setups are considered and the associated OTF presented. Confocal interferometric microscopy, for example forms the basis of optical coherence systems (such as optical coherence tomography (OCT)), whilst a coherence probe microscope (CPM) is an example of a conventional interference microscope [77] commonly found in surface profilometry [78].

To derive the OTF for interferometric imaging it must first be noted that the intensity at a point \mathbf{r}_2 in detector space is given by

$$I_i(\mathbf{r}_2) = |E_d(\mathbf{r}_2)|^2 + |E_{ref}(\mathbf{r}_2)|^2 + 2\Re[E_d(\mathbf{r}_2)E_{ref}^*(\mathbf{r}_2)], \quad (32)$$

where $E_{ref}(\mathbf{r}_2)$ is the reference field (and the dependence on \mathbf{r}_s has been omitted for clarity). Three contributions can be identified namely two non-interference terms arising from the object and reference beam, plus a term from the interference of the object and reference field. For simplicity, it will be assumed that in the reference arm the scattering function is given by a complex constant, r , as appropriate to reflection by a mirror, i.e. $t_{ref}(\mathbf{r}_1) = r\delta(z_1)$. Note the associated spectrum is $\tilde{t}_{ref}(\mathbf{m}) = r\delta(m)\delta(n)$. For a general detection geometry, the measured reference intensity is given, in analogy

with (16), by

$$I_{\text{ref}}(\mathbf{r}_s) = \iint \tilde{H}_{\text{ref}}(\mathbf{m}, \mathbf{m}') \tilde{t}_{\text{ref}}(\mathbf{m}) \tilde{t}_{\text{ref}}^*(\mathbf{m}') d\mathbf{m} d\mathbf{m}' \quad (33)$$

$$= |r|^2 \iint \tilde{H}_{\text{ref}}(0, 0, q, 0, 0, q') dq dq'. \quad (34)$$

It is noted that the reference object is not scanned such that there is no dependence on \mathbf{r}_s . Here, in analogy with (17),

$$\tilde{H}_{\text{ref}}(\mathbf{m}, \mathbf{m}') = \int \tilde{h}_{\text{eff-ref}}(\mathbf{m}, \mathbf{r}_2) \tilde{h}_{\text{eff-ref}}^*(\mathbf{m}', \mathbf{r}_2) D(\mathbf{r}_2) d\mathbf{r}_2 \quad (35)$$

and $\tilde{h}_{\text{eff-ref}}(\mathbf{m}, \mathbf{r}_2)$ is defined analogously to equation (14) albeit with the pupil functions replaced by those appropriate for the reference arm optics.

Most interesting, however, are the interference terms since these carry information about the object. The point-wise intensity in detector space is given by a term of the form

$$E_d(\mathbf{r}_2) E_{\text{ref}}^*(\mathbf{r}_2) = r^* \iint \tilde{h}_{\text{eff}}(\mathbf{m}, \mathbf{r}_2) \tilde{h}_{\text{eff-ref}}^*(0, 0, q', \mathbf{r}_2) \tilde{t}(\mathbf{m}) \times e^{2\pi i \mathbf{r}_s \cdot \mathbf{m}} d\mathbf{m} dq'. \quad (36)$$

The recorded intensity for each scan point is then given by

$$I_{\text{int}}(\mathbf{r}_s) = \int 2\Re[E_d(\mathbf{r}_2) E_{\text{ref}}^*(\mathbf{r}_2) D(\mathbf{r}_2) d\mathbf{r}_2] \quad (37)$$

$$= 2\Re \left[\int \tilde{h}_{\text{int}}(\mathbf{m}) \tilde{t}(\mathbf{m}) \exp[2\pi i \mathbf{r}_s \cdot \mathbf{m}] d\mathbf{m} \right], \quad (38)$$

where $\tilde{h}_{\text{int}}(\mathbf{m})$ is the interference CTF given by

$$\tilde{h}_{\text{int}}(\mathbf{m}) = r^* \iint \tilde{h}_{\text{eff}}(\mathbf{m}, \mathbf{r}_2) \tilde{h}_{\text{eff-ref}}^*(0, 0, q', \mathbf{r}_2) D(\mathbf{r}_2) d\mathbf{r}_2 dq'. \quad (39)$$

Given these equations it is apparent that interferometric systems represent a different class of system to both coherent and incoherent systems. Specifically it is important to note, as evident from equation (37), that the recorded intensity I_{int} is linearly dependent on the scattering potential $t(\mathbf{r})$, in contrast to the linear relationships detailed previously for coherent and incoherent systems. Since, detectors record the incident intensity, yet it is the (potentially complex) scattering potential that is sought in optical metrology; interferometry based configurations are the more popular in this context.

2.5. Monochromatic versus polychromatic illumination

Thus far consideration has been restricted to a monochromatic treatment; however, numerous polychromatic metrology techniques exist, such as OCT, coherence scanning interferometry (CSI), confocal chromatic microscopy (CCM) and dispersive scanning interferometry (DSI) [2]. Implicit in the earlier results is a dependence on the illumination wave, via $k = 2\pi/\lambda$. It is possible to define a polychromatic transfer function by integrating the monochromatic transfer function [79–84]; however, this approach is only valid under the assumption that the object function $t(\mathbf{r})$ is itself not dependent on the wavelength. Given the usual definition of the scattering potential in section 2.1, it is evident that this does not hold, due to a dependence on both illumination wavenumber k and refractive index. The k^2 factor in the scattering potential can however be absorbed into the appropriate expressions for

the transfer function (see e.g. [85]). Such an approach will naturally accommodate chromatic aberrations and dispersive effects of the measurement system. Dispersive effects of the sample may, however, exist as will be parameterized within the refractive index term of the scattering potential. Assuming, however, that no strong material resonances exist within the illumination bandwidth, these effects will be weak. These conditions are assumed to apply here, so that a polychromatic CTF may be defined as

$$\tilde{h}_{\text{poly}}(\mathbf{m}, \mathbf{r}_2) = \int \tilde{h}_{\text{mono}}(\mathbf{m}, \mathbf{r}_2, \lambda) s(\lambda) d\lambda, \quad (40)$$

where $s(\lambda)$ represents the (complex) amplitude of each spectral component. Accordingly the polychromatic TCC follows as

$$\tilde{H}_{\text{poly}}(\mathbf{m}, \mathbf{m}') = \iint \iint \tilde{h}_{\text{mono}}(\mathbf{m}, \mathbf{r}_2, \lambda) \tilde{h}_{\text{mono}}^*(\mathbf{m}', \mathbf{r}_2, \lambda') \times \langle s(\lambda) s^*(\lambda') \rangle D(\mathbf{r}_2) d\lambda d\lambda' d\mathbf{r}_2, \quad (41)$$

where the angular brackets, $\langle \cdot \cdot \rangle$, denote temporal averaging. If strong phase coherence is present between spectral components, then $\langle s(\lambda) s^*(\lambda') \rangle = s(\lambda) s^*(\lambda')$. Conversely for a temporally incoherent source, such as an incandescent lamp $\langle s(\lambda) s^*(\lambda') \rangle = S(\lambda) \delta(\lambda - \lambda')$ such that

$$\tilde{H}_{\text{poly}}(\mathbf{m}, \mathbf{m}') = \int R(\lambda) \tilde{H}_{\text{mono}}(\mathbf{m}, \mathbf{m}', \lambda) S(\lambda) d\lambda, \quad (42)$$

where the spectral response $R(\lambda)$ of the detector has also been introduced for completeness and $\tilde{H}_{\text{mono}}(\mathbf{m}, \mathbf{m}', \lambda)$ is the monochromatic TCC discussed in earlier sections. Ultimately the image intensity is given once more by equation (17) with use of the polychromatic TCC instead of the monochromatic TCC. Care must however be taken in employing the polychromatic version of equation (17) due to the underlying assumption of shift invariance required in the definition of a transfer function. Particularly, whilst shift-invariance may hold for each spectral component individually, this in itself does not guarantee that the polychromatic image will be shift invariant. Considering the basic imaging equations it can be seen that polychromatic shift invariance will not hold if the magnification of the imaging system is strongly wavelength dependent [80]. Further dangers of using polychromatic transfer functions, arising from the possibility of non-uniqueness, have been highlighted in [86].

2.6. Surface topography measurements

Whilst surface topography measurements represent a class of 3D imaging measurements in a broad sense, and are hence describable (under the correct conditions) by the framework given thus far, they are a special class. Accordingly further results may be expected to follow within this field of study. This is indeed true, as can be seen upon a re-examination of scattering from surfaces as is presented here.

Fundamentally when a surface is illuminated by a single plane wave, a spectrum of output plane waves can result. Surface scattering is therefore commonly formulated using a scattering function $\tilde{S}(\mathbf{m}_1; \mathbf{m}_2)$ which describes the relative amplitude and phase between an input plane wave propagating

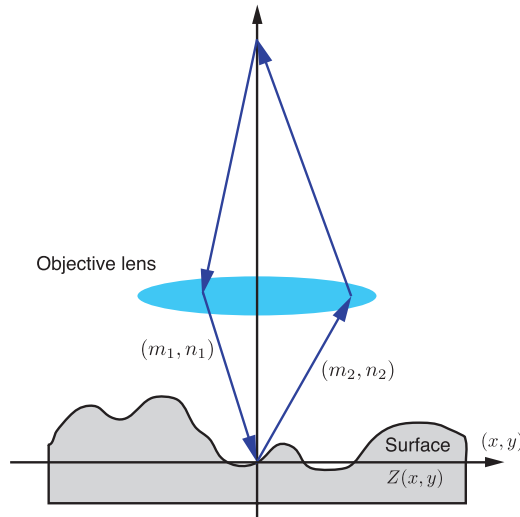


Figure 3. Simplified geometry of surface measurement depicting an incident plane wave with direction defined by (m_1, n_1) scattered to a plane wave with direction (m_2, n_2) .

in a direction defined by the direction cosines \mathbf{m}_1 and one of the output plane waves propagating in a direction defined by the direction cosines \mathbf{m}_2 [87] (see figure 3). If, however, the radius of curvature at each point on the surface can be considered to be much greater than the wavelength, then the surface can be considered to be locally plane, such that a single input plane wave gives rise to a single output plane wave dependent on the tilt of the surface. Under these circumstances, it is logical to change coordinate systems to $\mathbf{m} = \mathbf{m}_1 - \mathbf{m}_2$, where it is also noted that \mathbf{m} represents the spatial frequency components of the surface. This is known as the Kirchoff approximation [88]. Under this approximation, the scattering function can be written in the form $\tilde{S}(\mathbf{m})$. Such a replacement is also possible if the surface height variations are small [87]. The image amplitude following scattering from the surface can then be written in the form

$$E_d(\mathbf{r}_s, \mathbf{r}_2) = \int \tilde{h}_{\text{eff}}(\mathbf{m}, \mathbf{r}_2) \tilde{S}(\mathbf{m}) \exp[2\pi i \mathbf{r}_s \cdot \mathbf{m}] d\mathbf{m} \quad (43)$$

which should be compared with equation (13).

Provided that the surface is smooth at the optical scale and there is negligible multiple scattering, the 3D object can be replaced by an infinitely thin ‘foil’ like object placed at the interface [89]. Indeed, using this model, it has been shown that for a 1D perfectly conducting surface, illuminated by *s*-polarized light, the scattering function can be written in the form [88]

$$\tilde{S}(m, q) = \left(\frac{m^2 + q^2}{2q} \right) \int \exp[-2\pi i(mx + qZ(x))] dx. \quad (44)$$

This result was later extended to 2D surfaces [87] and reads

$$\begin{aligned} \tilde{S}(\mathbf{m}) &= \frac{|\mathbf{m}|^2}{2q} \iint \exp[-2\pi i(mx + ny + qZ(x, y))] dx dy \\ &= \frac{|\mathbf{m}|^2}{2q} \int \delta(z - Z(x, y)) \exp[-2\pi i \mathbf{m} \cdot \mathbf{r}] d\mathbf{r} \\ &= \frac{|\mathbf{m}|^2}{2q} \tilde{t}(\mathbf{m}), \end{aligned} \quad (45)$$

where from equation (45) it can be seen that the object spectrum $\tilde{t}(\mathbf{m})$ is the 3D Fourier transform of the surface profile. The geometric pre-factor introduced when considering surface scattering reduces to unity for low numerical aperture systems. Equations (13), (43) and (45) show that for surface measurements the effective CTF becomes

$$\tilde{h}_{\text{eff-sur}}(\mathbf{m}) = \frac{|\mathbf{m}|^2}{2q} \tilde{h}_{\text{eff}}(\mathbf{m}). \quad (46)$$

Earlier expressions derived for coherent, incoherent, partially coherent and interferometric imaging systems are all dependent on the CTF $\tilde{h}_{\text{eff}}(\mathbf{m})$ when imaging 3D objects. Given equation (46) these results are still applicable with the replacement $\tilde{h}_{\text{eff}}(\mathbf{m}) \rightarrow \tilde{h}_{\text{eff-sur}}(\mathbf{m})$ in the appropriate formulae.

3. Measurement of 3D transfer functions

The first part of this report has focused on laying out the theory of transfer functions in optical imaging systems. Formulations of this nature were pursued with a view to calibration of metrology systems. It has long been recognized that such a calibration and characterization of measurement systems can be obtained by measurement of either the 3D PSF or the associated OTF [90, 91]. This has become increasingly sought as measurement protocols have moved away from more traditional parameters, such as surface roughness or form, towards measuring the full power spectral density of a 3D object or surface [92–95]. Accordingly, the latter portion of this review turns attention to the measurement of the transfer function of optical imaging and interferometric setups. Due to the relationships expounded above between the 3D PSF and the 3D OTF, direct measurement of the PSF can also be considered as a measurement of the OTF in some (but not all) cases.

Given the assortment of imaging setups possible, distinction must be made as to which transfer function is to be measured. For example, if a confocal reflection microscope is used for surface profiling [96] calibration requires measurement of the complex CTF, whilst for a confocal interferometric setup the interference CTF must instead be measured [76]. Alternatively, in a spatially incoherent system, the OTF is required. Different measurement procedures must hence be pursued in each case and care taken in selecting the appropriate acquisition and processing technique.

To highlight this issue consider first the possible forms of the imaging equations, expressed in terms of the relevant transfer function, which are stated here for clarity. Specifically for a spatially fully, partially and in-coherent setup the imaging equations are

$$I_{\text{coh}}(\mathbf{r}_s) = \left| \int \tilde{h}(\mathbf{m}) \tilde{t}(\mathbf{m}) \exp[2\pi i \mathbf{r}_s \cdot \mathbf{m}] d\mathbf{m} \right|^2 \quad (47)$$

$$\begin{aligned} I_{\text{pc}}(\mathbf{r}_s) &= \iint \tilde{H}(\mathbf{m}, \mathbf{m}') \tilde{t}(\mathbf{m}) \tilde{t}^*(\mathbf{m}') \\ &\quad \times \exp[2\pi i \mathbf{r}_s \cdot (\mathbf{m} - \mathbf{m}')] d\mathbf{m} d\mathbf{m}' \end{aligned} \quad (48)$$

$$I_{\text{inc}}(\mathbf{r}_s) = \int \tilde{H}(\mathbf{m})\tilde{T}(\mathbf{m}) \exp[2\pi i\mathbf{r}_s \cdot \mathbf{m}] \, d\mathbf{m} \quad (49)$$

respectively where the separability of the TCC in the coherent case has been emphasized. Supplementing these equations with that of an interferometric setup, i.e.

$$I_{\text{int}}(\mathbf{r}_s) = 2\Re \left[\int \tilde{h}(\mathbf{m})\tilde{t}(\mathbf{m}) \exp[2\pi i\mathbf{r}_s \cdot \mathbf{m}] \, d\mathbf{m} \right] \quad (50)$$

yields the complete set of equations to be considered. Following the discussion in section 2.5 it is noted that the OTFs of equations (47)–(50) may be either monochromatic or polychromatic as appropriate for the system under study. Before existing literature on the measurement of the transfer function is reviewed, it is important to mention that many such works aim to measure only a 2D transfer function. Given equation (11) (and its analogue for the other system geometries under consideration) it is evident that all such techniques can be employed for the measurement of the 2D defocused transfer function, by introducing a variable defocus of the test object into the system, such that a 3D image stack can be acquired to ultimately enable the reconstruction of the full 3D OTF. Measurements of 2D transfer functions will hence also be included within the following review.

3.1. Incoherent systems

Solution of the imaging equations for the transfer function is simplest for an incoherent system and hence considered first. In this case, equation (49), or equivalently equation (30), holds. Solution for the OTF then quickly follows by taking the ratio of a measured image spectrum obtained from a known object with the spectrum of the object distribution, i.e.

$$\tilde{H}(\mathbf{m}) = \tilde{I}(\mathbf{m})/\tilde{T}(\mathbf{m}). \quad (51)$$

The majority of techniques to experimentally measure the OTF were developed during the 1940s–1960s [30, 91], many based on this approach. Knowledge of the form of the sample object is however crucial to an accurate determination of the OTF. Moreover, judicious choice of the sample object must be made so as to avoid zeros in its spectrum, in turn implying the transfer function cannot be determined over a complete range of frequencies. Historically, a plethora of alternative structures and standard targets have indeed been employed in the measurement of the OTF each with their own merits. Many works, however, only aim to measure the MTF. Whilst the MTF by itself does not contain complete information about the optical system, it is often sought if only a parameter derived from the full image data, such as surface height, is available instead of the image data itself [97], as may be true for commercial systems. In this case, it is more appropriate to say that it is the instrument transfer function which is sought; however, there is no guarantee that intermediate processing steps include solely linear operations as required for a transfer function description to be valid. Alternatively, an implicit assumption that the PSF is symmetric (and hence an even function) is made, in turn yielding a purely real OTF. This latter assumption must, however, be viewed with caution since it will not hold in general, especially for an aberrated system.

Equation (29) encapsulates perhaps the most intuitive method by which the OTF in an incoherent system can be measured. In particular, if a point object is used as a test object, the acquired image can be directly Fourier transformed to give the complete complex OTF, from which the MTF and PTF can easily be found. Equivalently this can be seen from equation (51) since the 3D spectrum of an ideal point object (mathematically represented by a Dirac delta function) is a uniform, isotropic distribution, i.e. $\tilde{T}(\mathbf{m}) = 1$ for all \mathbf{m} . True sources, however, possess a finite size in turn introducing a frequency dependence in the object spectrum (albeit a weak dependence). If however $r_0 \ll \lambda/4$, then the object spectrum is approximately uniform such that the source can be considered effectively as a point [98]. It should nevertheless be noted that small scatterers do not scatter isotropically and have radii of curvature much smaller than the wavelength and thus break the conditions of validity of both the Kirchoff and Born approximation. Measurement of the PSF has however received much attention, particularly due to the availability of small fluorescent objects such as fluorescent microspheres (beads), fluorescent molecules or quantum dots, that represent effective point sources due to their size. 3D measurements of the intensity PSF have hence been made by authors such as Agard *et al* [99], Gibson and Lanni [100], and Goodwin [101]. Hiraoka *et al* similarly collect a series of 2D defocused images of the intensity PSF from which they proceed to calculate the OTF [102]. Protocols have further been developed to measure the intensity PSF of a confocal fluorescence microscope [103, 104]. Measurements obtained using CCDs are however limited by pixel size, as such Rhodes *et al* measure the intensity PSF of a lens directly using a near field probe [105]. Given that a point source is inherently spatially coherent any measured amplitude PSF determined via coherent detection (see section 3.2) can be used to find the intensity PSF (by taking the modulus and squaring cf equations (27) and (28)) appropriate to use of the imaging setup in an incoherent modality. In this vein, Beverage *et al* use a Shack–Hartmann sensor to measure the complex wavefront in the exit pupil of a 3D microscope [106]. The associated intensity PSF is then given by the modulus squared of the Fourier transform of the measured field distribution.

PSF measurements, however, can suffer significantly from low signal-to-noise ratios. Today rapid data acquisition permits multiple measurements to be obtained and averaged, hence improving signal to noise ratios. Furthermore, highly sensitive detectors exist which can help mitigate this issue to some extent; however, the use of a line object or knife edge inherently increases the energy transmitted, and hence the signal-to-noise ratio, by an order of magnitude [107]. The image of a line object is known as the line spread function (LSF), whilst that of an edge is the edge spread function (ESF), with the former given by the derivative of the latter [108–110]. In one dimension, the OTF is given by the 1D inverse Fourier transform of the LSF, a fact exploited by many authors [111–113]. However, to obtain a 2D coverage of frequency space it becomes necessary to rotate the object, so as to introduce an azimuthal dependence [112]. Algorithms for direct determination of the OTF from the ESF have been

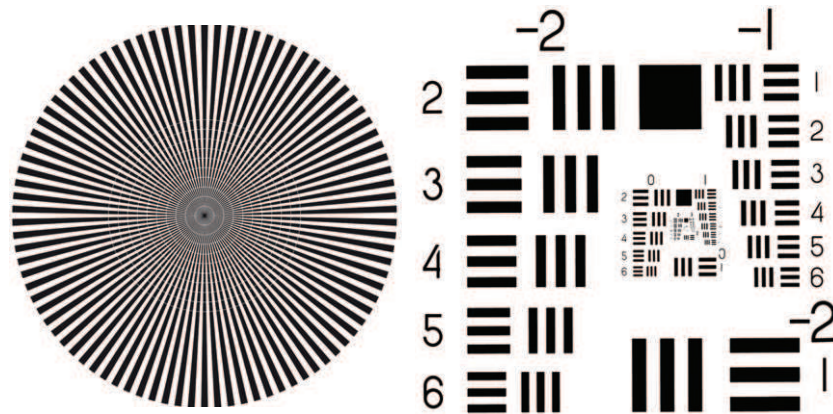


Figure 4. (left) Siemens star target and (right) USAF 1951 resolution target.

explored in [108, 114] and are preferable over a line object based method, since the latter suffers from the finite width of the object, in a similar fashion to that discussed for a finite sized point source above. It should be noted that modern targets, such as the ISO 12233 target, still include knife-edge type objects to enable OTF measurements via this method. A comparison of OTF measurements using the edge technique and interferometric methods is presented in [115], wherein it is concluded that they perform comparably, albeit the edge method can be less accurate at low frequencies. Whilst the techniques listed above measure the 2D OTF, step like or spherical objects, being inherently 3D in nature, allow for more direct measurement of the 3D OTF [30, 116, 117].

Given the physical meaning of the OTF, a further intuitive choice of the test object is that of a 3D sinusoidal grating. Since the spectrum of such an object ideally constitutes a single spatial frequency, equation (51) implies that the image spectrum directly yields the appropriate element of the OTF. In the context of sine wave targets, it is common to find studies in which only the MTF is measured. Specifically, instead of calculating the Fourier transforms implied in equation (51), the MTF is directly calculated by taking the ratio of the modulation (or contrast), defined as

$$M = \frac{I_{\max} - I_{\min}}{I_{\max} + I_{\min}}, \quad (52)$$

where I_{\max} and I_{\min} are the maximum and minimum intensities, in the final image and object distribution, i.e. $MTF = M_{\text{img}}/M_{\text{obj}}$. Such a technique however is limited since only a single spatial frequency can be probed for a single target. Targets were hence quickly developed in which the spatial frequency of the pattern varied spatially across the extent of the object. The original sine wave tests of Selwyn [33] have already been mentioned; however, this strategy was also pursued by other authors [118, 119], and still forms the basis of existing methods for more complicated systems [120, 121]. Fabrication of accurate sine wave gratings can however pose technical problems. Whilst in more recent years this has been overcome, for example by using the interference pattern formed from two (or more) plane waves to form a suitable grating [121] or modern lithographic procedures, originally the idea developed

to employ square wave [107, 122], or even triangular [123] test patterns due to the relative ease with which they could be made. It should also be noted that such targets cover more of the spatial frequency domain in a single image. More modern targets include the Siemens star target [124], Ronchi rulings and the USAF 1951 resolution target [125] (see figure 4).

A further class of 3D test object has been proposed, namely that of (pseudo-) random gratings [126], which has seen little attention until more recently [127–129]. Such a choice is motivated by the uniform power spectrum possessed by a pseudo-random grating. Furthermore, such gratings can be generated so as to possess shift-invariance, a property which has been shown to be locally violated in systems in which the image is sampled [130–132]. This technique furthermore improves the accuracy over those based on LSF/ESF measurements since high accuracy in these can only be achieved by using very narrow slits, which compromises signal levels [126]. The work detailed in [97, 133–138] similarly uses pseudo-random gratings (made via a standard lithographic process) as a test object, but here it is the MTF of the entire system, including effects from signal processing, detector response and environmental factors (as opposed to just the image forming optics), that is being measured. Polychromatic measurements of the MTF have also been made in [139, 140] by considering finite spectral bands, from which the polychromatic transfer function is subsequently calculated or directly measured [141, 142].

3.2. Coherent systems

Coherent systems (described by equation (47)) can be calibrated by measurement of their CTF. Many parallels can be drawn between the measurement of the CTF in a coherent system and of an OTF in incoherent systems, albeit the discussion must proceed in terms of complex field amplitude instead of intensity, such that

$$\tilde{h}(\mathbf{m}) = \tilde{E}_d(\mathbf{m})/\tilde{r}(\mathbf{m}), \quad (53)$$

where $\tilde{E}_d(\mathbf{m})$ is the spectrum of the detected complex field amplitude. Accordingly, an additional layer of difficulty is

introduced since complete measurements of the field must measure both field amplitude and phase. Whilst the former can be found by taking the square root of an intensity image, the latter requires use of, say, a wavefront sensor or interferometer.

Following the structure of section 3.1, consideration is first given to the measurement of the amplitude PSF. To maintain phase coherence between the illumination beam and the collected scattered field, fluorescent sources can no longer be used for such a measurement. A number of solutions have been proposed in this vein, with Schrader *et al.*, for example, using 80 nm diameter colloidal gold particles immersed in immersion oil [143] (although phase was not measured by the authors). Cotte *et al.* use a 75 nm diameter nano-hole created via focused ion beam milling [144]. As with the measurements of the intensity PSF, the finite size of these sources will play a role in accurate determination of the OTF.

By far the most common method to measure the complex field amplitude is via interferometry as was first proposed within the context of OTF measurements by Hopkins [145] (albeit within a partially coherent context). Selligson [146] and Dandliker *et al.* [147] have used a Mach–Zehnder interferometer to measure the aberrations present in a lens by mapping the phase and intensity PSFs in the focal region of a lens. Similarly, Schrader and Hell [148], and Török and Kao [149] used Tywman–Green interferometers, whilst Juškaitis and Wilson [150] and Walford *et al.* [151] employed a fibre optic interferometer. Holographic measurements have also recently been reported [144, 152].

Despite the prevalence of interferometric methods, non-interferometric methods have been used for PSF measurements. For example, Beverage *et al.* have used a Shack–Hartmann sensor placed at the exit pupil of a microscope [106] from which the PSF can be found by a Fourier transform. Intensity only measurements can also be used if a phase retrieval algorithm is exploited [153, 154]. In this scenario, complexity of the optical setup is traded for additional noise amplification arising from the increased post-acquisition data processing.

Due to the difficulties of coherent detection in optical setups, such measurements are not common in the literature. That said both experimental and theoretical developments are well established in acoustic imaging in which the image formation process is analogous to that of optical systems [155, 156]. Within this domain both line and step functions have been used to determine the CTF of the imaging system [155, 157]. A theoretical study of spherical objects in a scanning confocal reflection acoustic microscope has been presented in [158, 159], whilst experimental measurements of the 2D defocused CTF are discussed in [157, 160, 161]. In these studies, it was shown that a non-planar scan along the surface of a large steel sphere gives the in-focus CTF, whilst with small shifts of the focal position similar arc-scans give the 2D defocused CTF. Accordingly, by forming 3D images near the top of the sphere the 3D CTF can be found. If considering measurement of the PTF only, then phase steps have also been shown to be suitable [162] for such measurements.

3.3. Partially coherent systems

Given that in partially coherent systems transmission of spatial frequencies must be described pairwise via a TCC (see equation (48)), measurement of such transmission characteristics becomes more involved. An approach based on algebraic division in the spatial frequency domain, as was adopted for coherent and incoherent systems alike, can no longer be pursued, since calculating the image spectrum via a Fourier transform yields only equal frequency values of the TCC, i.e. $\tilde{H}(\mathbf{m}, \mathbf{m})$. For a conventional system, it was shown earlier that the TCC is given by the autocorrelation of the pupil function (see equation (20)). Measurement of such an autocorrelation integral can be performed by the inspection of the interference patterns arising from two identical but mutually shifted versions of the field. The lateral shift is commonly referred to as a shear of the field, such that the measurement setup is known as a shearing interferometer. Such an interferometer for the determination of the autocorrelation of a field for OTF measurements was suggested by Hopkins [145] and first implemented in a Michelson-type geometry by Baker [163]. Variants of lateral shearing interferometers of this nature have since been proposed [164–170]. Setups in which rotating glass plates [171], double gratings [172, 173] and correlated partial diffusers [174] introduce the necessary shear between fields have also been developed. A scanning setup has also been proposed in [175].

3.4. Interferometric systems

As with partially coherent systems, measurement of the transfer function in interferometric systems requires a little more thought. Inspection of equation (50) highlights that once more a simple Fourier analysis does not directly yield the transfer function. The reason for this complication is that both the transfer function $\tilde{h}(\mathbf{m})$ and object spectrum $\tilde{t}(\mathbf{m})$ can be complex. For the object spectrum, this will particularly be the case if the object exhibits any absorption, as is particularly the case with metallic materials. Any phase aberrations present in either the reference or object arm of the interferometer will likewise give rise to imaginary parts of the PSF and hence the transfer function.

Many commercial interferometer setups furthermore include a ground glass diffuser so as to reduce coherent noise, specifically speckle, that can arise from stray reflections and scattering in the optics. Specifically the interference pattern is imaged onto a rotating diffuser, which is subsequently relayed by a zoom lens onto a detector. In this way, the interference image acts as an incoherent source for the relay optics, adding an additional step in the image formation process described by equation (49). This step shall, however, be neglected here for simplicity.

To establish how the transfer function of an interferometric imaging system can be determined, it is first observed that equation (50) can be rewritten in the form

$$I_{\text{int}}(\mathbf{r}_s) = 2 \int |\tilde{h}(\mathbf{m}')| |\tilde{t}(\mathbf{m}')| \cos[2\pi \mathbf{r}_s \cdot \mathbf{m}' + \Phi_h(\mathbf{m}') + \Phi_t(\mathbf{m}')] d\mathbf{m}', \quad (54)$$

where $\Phi_h(\mathbf{m})$ is the PTF and $\Phi_t(\mathbf{m})$ is the phase angle of the object spectrum. Taking the Fourier transform yields

$$\begin{aligned}\tilde{I}_{\text{int}}(\mathbf{m}) &= \int |\tilde{h}(\mathbf{m}')| |\tilde{t}(\mathbf{m}')| \\ &\quad \times \{ \exp[i\Phi_h(\mathbf{m}') + i\Phi_t(\mathbf{m}')] \delta(\mathbf{m}' - \mathbf{m}) \\ &\quad + \exp[i\Phi_h(\mathbf{m}') + i\Phi_t(\mathbf{m}')] \delta(\mathbf{m}' + \mathbf{m}) \} d\mathbf{m}' \quad (55) \\ &= \tilde{h}(\mathbf{m}) \tilde{t}(\mathbf{m}) + \tilde{h}^*(-\mathbf{m}) \tilde{t}^*(-\mathbf{m}). \quad (56)\end{aligned}$$

Due to the spatial frequency cutoffs of the transfer function [176, 177], equation (56) describes two separated copies of the product $\tilde{h}(\mathbf{m})\tilde{t}(\mathbf{m})$ (and its conjugate) in frequency space, such that one can be filtered as part of post-processing. The filtered spectrum is thus of the form $\tilde{I}_{\text{int-fil}}(\mathbf{m}) = \tilde{h}(\mathbf{m})\tilde{t}(\mathbf{m})$ such that the interference CTF is given by

$$\tilde{h}(\mathbf{m}) = \tilde{I}_{\text{int-fil}}(\mathbf{m}) / \tilde{t}(\mathbf{m}). \quad (57)$$

Indeed, such an approach has been adopted in [178, 179] upon acquisition of the PSF of the system using a coherence scanning interferometer. The MTF of an OCT system has also been reported in [180, 181], as determined through measurements of nanoparticles. Grid patterns have also been used to establish the PTF of a phase-shifting interferometer [182]. Novak *et al* have used both phase steps and sine wave structures for characterizing a Fizeau interferometer [121]. Yashchuk *et al* have shown that their proposed technique of using random gratings can be extended to measuring the MTF of interferometric systems, such as a Fizeau interferometer [137, 138]. An OTF measurement scheme, based on a shearing interferometer, using a white light source has also been proposed in [172] and is hence also suitable for study of white light interferometers or other polychromatic techniques.

4. Discussion

OTF theory covers an extensive array of optical systems ranging from spatially coherent to incoherent systems, monochromatic to white light sources and interferometric setups, yet it is the broad applicability and simplicity of the underlying principles which account for its success and prominence in the literature and beyond. Theoretical developments in this vein date back to before the invention of the laser, perhaps justifying the greater extent to which experimental studies have centered on partially coherent or incoherent setups. As optical technology has progressed, however, so has transfer function theory, with analytic expressions now available for many idealized optical configurations. Natural progression to the description of fully 3D systems is also clearly evident in the literature. Many practical systems are however far from ideal, yet despite this experimental measurement of transfer functions has seen slower development, especially for 3D imaging arrangements. Arguably such reticence likely follows from the greater ease with which alternative performance metrics, such as resolution, can be determined, e.g. by means of resolution targets. For many applications system characterization by such incomplete means has proved adequate, yet now with the movement towards formulation of optical metrological

standards, full system knowledge is required hence motivating accurate measurement of OTFs. Existing methods of performing OTF measurements have been reviewed in the latter portions of this text, however the question as to which method is preferred remains open. Predominantly, OTF measurements all follow the same principle, namely measure the 3D ‘image’ of an object with an accurately known spectrum (i.e. shape), from which the image spectrum and consequently the transfer function can be computed.

The question of optimality is not a trivial question to answer; however, the key principles of a good measurement are clearly identifiable. In particular, a good measurement should:

- (i) provide information across the full transmission bandwidth of the optical setup,
- (ii) be well-posed, i.e. contain no zeros in the object spectrum,
- (iii) be repeatable and robust,
- (iv) be simple to implement, so as to permit and promote easy uptake by industrial users,
- (v) require objects which can practically (and cheaply) be manufactured.

Given requirement (i), techniques which employ multiple targets, e.g. sine wave targets or line gratings can immediately be excluded since these constitute a discrete set of object frequencies and hence the full system bandwidth is not covered and information is consequently lost. Targets such as a Siemens stars are also not suitable, since these probe spatial frequencies in one direction only (in this case the azimuthal direction) with no regard to variations in the radial or axial direction. Care must hence be taken to ensure variations exist in all three dimensions of any test object. Requirement (ii) also directly precludes a number of targets. For example a square pillar, if chosen too large, will have zero crossings in its 3D spectrum which lie within the spatial bandwidth of the measuring system. Other examples of objects with zero crossings might include grooves. Such zeros inherently imply that no information regarding the value of the transfer function at the associated frequency is contained within the experimental data and hence solution is ill-posed.

Robustness (requirement (iii)) can be expressed in terms of the susceptibility of a measurement of a transfer function to noise. The first step to minimize the degrading effects of noise is to maximize the signal to noise ratio, by maximizing light throughput in the system. Point objects are undesirable for this reason (as well as the associated difficulty in their manufacture). Assuming experimental conditions are maintained (i.e. noise levels upon detection are constant) it is the post-processing of the raw image stack which will dominate overall noise properties on the inferred transfer function. Consider, for example, determining the OTF or CTF via equations (51) or (53) in which the experimental image is divided by the known object spectrum (an intuitive and mathematically simple procedure as may be preferred as per requirement (iv)). Any noise present on the image is amplified via division, with the frequencies which are present only weakly in the object suffering the worse noise amplification. A step artefact for example has a spectrum in which the amplitude falls off at higher frequencies, such that

the inferred transfer function would be corrupted by noise to a greater extent at higher frequencies. At best a uniform object spectrum is therefore chosen, hence suggesting the use of large spherical objects or random arrays. Of these it is arguably the former which is practically easier to manufacture (requirement (v)) within the tolerances demanded for industrial standards, however this has still to be realized in practice.

Acknowledgments

This work was funded by the BIS National Measurement System Engineering Measurement Programme 2011-2014 and the EPSRC Knowledge Transfer Secondment Scheme 2011. We also thank Rahul Mandal and Kanik Palodhi (University of Loughborough, UK) for their contributions.

References

- [1] Whitehouse D J 1994 *Handbook of Surface Metrology* (Bristol: Institute of Physics Publishing)
- [2] Leach R K (ed) 2011 *Optical Measurement of Surface Topography* (Berlin: Springer)
- [3] Whitehouse D J 1997 Surface metrology *Meas. Sci. Technol.* **8** 955–72
- [4] Leach R 2009 *Fundamental Principles of Engineering Nanometrology* (Amsterdam: Elsevier)
- [5] Schmaltz G 1929 Über Glätte und Ebenheit als physikalisches und physiologisches problem *Z. Vereines deutscher Ingenieure* **73** 1461–7
- [6] Tolansky S 1960 *Surface Microtopography* (New York: Wiley-Interscience)
- [7] Bennett J M 1976 Measurement of the rms roughness, autocovariance function and other statistical properties of optical surfaces using a FECO scanning interferometer *Appl. Opt.* **15** 2705–21
- [8] Miroshnikov M M 2010 Academician Vladimir Pavlovich Linnik—the founder of modern optical engineering (on the 120th anniversary of his birth) *J. Opt. Technol.* **77** 401–8
- [9] Bhushan B, Wyant J C and Koliopoulos C L 1985 Measurement of surface topography of magnetic tapes by Mirau interferometry *Appl. Opt.* **24** 1489–97
- [10] Creath K 1987 Step height measurement using two-wavelength phase-shifting interferometry *Appl. Opt.* **26** 2810–6
- [11] Lee B S and Strand T C 1990 Profilometry with a coherence scanning microscope *Appl. Opt.* **29** 3784–8
- [12] de Groot P and Deck L 1995 Surface profiling by analysis of white-light interferograms in the spatial frequency domain *J. Mod. Opt.* **42** 389–401
- [13] Hamilton D K and Wilson T 1982 Surface profile measurement using the confocal microscope *J. Appl. Phys.* **53** 5320–2
- [14] Leach R K, Giusca C L and Naoi K 2009 Development and characterisation of a new instrument for the traceable measurement of areal surface texture *Meas. Sci. Technol.* **20** 125102
- [15] Thomsen-Schmidt P 2011 Characterisation of a traceable profiler instrument for areal roughness measurement *Meas. Sci. Technol.* **22** 094019
- [16] Giusca C L, Leach R K and Forbes A B 2011 A virtual machine-based uncertainty evaluation for a traceable areal surface texture measuring instrument *Measurement* **44** 988–93
- [17] Giusca C L, Leach R K, Helery F, Gutauskas T and Nimishakavi L 2011 Calibration of the scales of areal surface topography measuring instruments: part 1. Measurement noise and residual flatness *Meas. Sci. Technol.* **23** 035008
- [18] Giusca C L, Leach R K and Helery F 2012 Calibration of the scales of areal surface topography measuring instruments: part 2. Amplification, linearity and squareness *Meas. Sci. Technol.* **23** 065005
- [19] Giusca C L, Leach R K, Helery F and Gutauskas T 2011 Calibration of the geometrical characteristics of areal surface topography measuring instruments *J. Phys.: Conf. Ser.* **311** 012005
- [20] www.ptb.de/de/org/5/51/511/doc/calibration_artefacts.pdf
- [21] www.nanoscale.de/standards.htm
- [22] www.nist.gov
- [23] Wilkening G and Koenders L (ed) 2005 *Nanoscale Calibration Standards and Methods* (New York: Wiley)
- [24] Krüger-Sehm R, Hässler-Grohne W and Fruehauf J 2004 Traceable calibration standard for lateral axis of stylus instruments *Wear* **257** 1241–5
- [25] Fujii A, Suzuki H and Yanagi K 2011 Development of measurement standards for verifying functional performance of surface texture measuring instruments *J. Phys.: Conf. Ser.* **311** 012009
- [26] Church E L and Takacs P Z 1989 Effects of optical transfer function in surface profile measurements *Proc. SPIE* **1164** 46–50
- [27] de Groot P and de Lega X C 2006 Interpreting interferometric height measurements using the instrument transfer function *Proc. Fringe* 2005 pp 30–37
- [28] Foreman M R, Coupland J M, Giusca C L and Leach R K 2012 Determination of the transfer function for optical surface topography measuring instruments *Technical Report ENG36*, National Physical Laboratory, UK
- [29] Williams T 1998 *The Optical Transfer Function of Imaging Systems* (Bristol: Institute of Physics Publishing)
- [30] Williams C S and Becklund O A 2002 *Introduction to the Optical Transfer Function* (Bellingham, WA: SPIE Optical Engineering Press)
- [31] Gu M 1996 *Principles of Three-Dimensional Imaging in Confocal Microscopes* (Singapore: World Scientific)
- [32] Duffieux P M 1946 *L'intégrale de Fourier et ses applications a l'Optique* (Rennes)
- [33] Selwyn E W H and Tearle J L 1946 *Proc. Phys. Soc.* **58** 493–525
- [34] Gu M, Gan X and Sheppard C J R 1991 Three-dimensional coherent transfer functions in fiber-optical confocal scanning microscopes *J. Opt. Soc. Am. A* **8** 1019–25
- [35] Nakamura O and Kawata S 1990 Three-dimensional transfer-function analysis of the tomographic capability of a confocal fluorescence microscope *J. Opt. Soc. Am. A* **7** 522–6
- [36] Streibl N 1985 Three dimensional imaging by a microscope *J. Opt. Soc. Am. A* **2** 121–7
- [37] Goodman J W 1996 *Introduction to Fourier Optics* 2nd edn (New York: McGraw-Hill)
- [38] Sheppard C J R and Mao X Q 1989 Three dimensional imaging in a microscope *J. Opt. Soc. Am. A* **6** 1260–9
- [39] Dändliker R and Weiss K 1970 Reconstruction of the three-dimensional refractive index from scattered waves *Opt. Commun.* **1** 323–8
- [40] Wolf E 1969 Three-dimensional structure determination of semi-transparent objects from holographic data *Opt. Commun.* **1** 153–6
- [41] Frieden B R 1967 Optical transfer of the three-dimensional object *J. Opt. Soc. Am.* **57** 56–66
- [42] Hopkins H H 1953 On the diffraction theory of optical images *Proc. R. Soc. A* **217** 408–32
- [43] Sheppard C J R and Choudhury A 1977 Image formation in the scanning microscope *Opt. Acta* **24** 1051–73

- [44] Hopkins H H 1955 The frequency response of a defocused optical system *Proc. R. Soc. A* **231** 91–103
- [45] Sheppard C J R, Hamilton D K and Cox I J 1983 Optical microscopy with extended depth of field *Proc. R. Soc. A* **387** 171–86
- [46] Sheppard C J R and Wilson T 1978 Image formation in scanning microscopes with partially coherent source and detector *Opt. Acta* **25** 315–25
- [47] Sheppard C J R and Wilson T 1980 Fourier imaging of phase information in scanning and conventional optical microscopes *Phil. Trans. R. Soc. London* **295** 513–36
- [48] Sheppard C J R and Wilson T 1981 The theory of the direct-view confocal microscope *J. Microsc.* **124** 107–17
- [49] Wilson T and Sheppard C 1984 *Theory and Practice of Scanning Optical Microscopy* (London: Academic)
- [50] Sheppard C J R, Gu M and Mao X G 1978 Three-dimensional coherent transfer function in a reflection mode confocal scanning microscope *Opt. Commun.* **25** 281–4
- [51] Sheppard C J R and Gu M 1991 Three-dimensional optical transfer function for an annular lens *Opt. Commun.* **81** 276–80
- [52] Gu M and Sheppard C J R 1992 Three-dimensional optical transfer function in the fibre-optical confocal scanning microscope using annular lenses *J. Opt. Soc. Am. A* **9** 1991–9
- [53] Gu M and Sheppard C J R 1992 Three-dimensional coherent transfer function in reflection-mode confocal microscopy using annular lenses *J. Mod. Opt.* **39** 783–93
- [54] Gu M and Sheppard C J R 1993 Three-dimensional coherent transfer functions in confocal imaging with two unequal annular lenses *J. Mod. Opt.* **40** 1255–72
- [55] Sheppard C J R, Gu M, Kawata Y and Kawata S 1994 Three-dimensional transfer functions for high aperture systems *J. Opt. Soc. Am. A* **11** 593–8
- [56] Gu M and Sheppard C J R 1992 Effects of defocus and primary spherical aberration on three-dimensional coherent transfer functions in confocal microscopes *Appl. Opt.* **31** 2541–9
- [57] Drazic V 1992 Dependence of two- and three-dimensional optical transfer functions on pinhole radius in a coherent confocal microscope *J. Opt. Soc. Am. A* **9** 725–31
- [58] Born M and Wolf E 1980 *Principles of Optics* 7th edn (Cambridge: Cambridge University Press)
- [59] Sheppard C J R and Matthews H J 1987 Imaging in high-aperture optical systems *J. Opt. Soc. Am. A* **4** 1354–60
- [60] Sheppard C J R and Gu M 1993 Imaging by a high aperture optical system *J. Mod. Opt.* **40** 1631–51
- [61] Sheppard C J R, Gannaway J N and Choudhury A 1977 Electromagnetic field near the focus of wide-angular annular lens and mirror systems *Microw. Opt. Acoust.* **1** 129–32
- [62] Urbańczyk W 1982 Optical imaging in polarised light *Optik* **63** 25–35
- [63] Urbańczyk W 1984 Optical imaging systems changing the state of light polarization *Optik* **66** 301–9
- [64] Urbańczyk W 1986 Optical transfer functions for imaging systems which change the state of light polarization *Opt. Acta.* **33** 53–62
- [65] Arnison M R and Sheppard C J R 2002 A 3D vectorial optical transfer function suitable for arbitrary pupil functions *Opt. Commun.* **211** 53–63
- [66] Sheppard C J R and Larkin K G 1997 Vectorial pupil functions and vectorial transfer functions *Optik* **107** 79–87
- [67] Jackson J D 1998 *Classical Electrodynamics* (New York: Wiley)
- [68] Trattner S, Feigin M, Greenspan H and Sochen N 1981 Validity criterion for the Born approximation convergence in microscopy imaging *J. Microsc.* **124** 107–17
- [69] Malacara D (ed) 2007 *Optical Shop Testing* 3rd edn (New York: Wiley)
- [70] Török P and Kao F-J (ed) 2007 *Optical Imaging and Microscopy—Techniques and Advanced Systems* 2nd edn (New York: Springer)
- [71] Brakenhoff G J 1979 Imaging modes in confocal scanning light microscopy *J. Microsc.* **117** 233
- [72] Wilson T and Juškaitis R 1994 Scanning interference microscopy *Bioimaging* **2** 36–40
- [73] Ojeda-Castañeda J and Jara E 1980 Transfer function with quadratic detection: coherent illumination *J. Opt. Soc. Am.* **70** 458–61
- [74] Kou S S and Sheppard C J R 2007 Imaging in digital holographic microscopy *Opt. Express* **15** 13640–8
- [75] Kou S S and Sheppard C J R 2008 Image formation in holographic tomography *Opt. Lett.* **33** 2362–4
- [76] Quartel J and Sheppard C J R 1996 A surface reconstruction algorithm based on confocal interferometric profiling *J. Mod. Opt.* **43** 591–605
- [77] Davidson M, Kaufman K and Mazor I 1987 The coherence probe microscope *Solid State Technol.* **730** 57–59
- [78] Sheppard C J R, Roy M and Sharma M D 1978 Image formation in low-coherence and confocal interference microscopes *Appl. Opt.* **25** 1493–502
- [79] Subbarao M 1990 Optical transfer function of a diffraction-limited system for polychromatic illumination *Appl. Opt.* **29** 554–8
- [80] Barnden R 1974 Calculation of axial polychromatic optical transfer function *Opt. Acta* **21** 981–1003
- [81] Barnden R 1976 Extra-axial polychromatic optical transfer function *Opt. Acta* **23** 1–24
- [82] Navajas D, Vallmitjana S, Barandalla J J and Moneo J R de F 1982 Evaluation of polychromatic image quality by means of transfer function *J. Opt.* **13** 283
- [83] Chakraborty B 1988 Polychromatic optical transfer function of a perfect lens masked by birefringent plates *J. Opt. Soc. Am. A* **5** 1207–12
- [84] de Groot P and de Lega X C 2004 Signal modelling for low-coherence height-scanning interference microscopy *Appl. Opt.* **43** 4821–30
- [85] Coupland J M and Lobera J 2008 Holography, tomography and 3D microscopy as linear filtering operations *Meas. Sci. Technol.* **19** 074012
- [86] Takeda M 1981 Chromatic aberration matching of the polychromatic optical transfer function *Appl. Opt.* **20** 684–7
- [87] Sheppard C J R, Connolly T J and Gu M 1993 Imaging and reconstruction for rough surface scattering in the Kirchhoff approximation by confocal microscopy *J. Mod. Opt.* **14** 2407–21
- [88] Beckmann P and Spizzichino A 1987 *The Scattering of Electromagnetic Waves from Rough Surfaces* (Norwood, MA: Artech House)
- [89] Mandal R, Palodhi K, Coupland J, Leach R K and Mansfield D 2012 Application of linear systems theory to characterize coherence scanning interferometry *Proc. SPIE* **8430** 84300T
- [90] Baker L (ed) 1992 *Selected papers on Optical Transfer Function: Foundation and theory (SPIE Milestone Series vol MS 59)* (Bellingham, WA: SPIE Optical Engineering Press)
- [91] Baker L (ed) 1992 *Selected papers on Optical Transfer Function: Measurement (SPIE Milestone Series vol MS 60)* (Bellingham, WA: SPIE Optical Engineering Press)
- [92] Church E L, Jenkinson H A and Zavada J M 1979 Relationship between surface scattering and microtopographic features *Opt. Eng.* **18** 125–36
- [93] Church E L and Berry H C 1982 Spectral analysis of the finish of polished optical surfaces *Wear* **83** 189–201

- [94] Elson J M and Bennett J M 1995 Calculation of the power spectral density from surface profile data *Appl. Opt.* **34** 201–8
- [95] Yashchuk V V, Franck A D, Irick S C, Howells M R, MacDowell A A and McKinney W R 2005 Two dimensional power spectral density measurements of x-ray optics with the micromap interferometric microscope *Proc. SPIE* **5858** 58580A
- [96] Udupa G, Singaperumal M, Sirohi R S and Kothiyal M P 2000 Characterization of surface topography by confocal microscopy: I. Principles and the measurement system *Meas. Sci. Technol.* **11** 305–14
- [97] Barber S K, Anderson E D, Cambie R, McKinney W R, Takacs P Z, Stover J C, Voronov D L and Yaschuk V V 2010 Binary pseudo-random gratings and arrays for calibration of modulation transfer function of surface profilometers *Nucl. Instrum. Methods A* **616** 172–82
- [98] van de Hulst H C 1981 *Light Scattering by Small Particles* (New York: Dover)
- [99] Agard D A, Hiraoka Y, Shaw P and Seday J W 1989 Fluorescence microscopy in three dimensions *Methods Cell Biol.* **30** 353–77
- [100] Gibson S F and Lanni F 1992 Experimental test of an analytical model of aberration in an oil-immersion objective lens used in three-dimensional light microscopy *J. Opt. Soc. Am. A* **9** 154–66
- [101] Goodwin P C 2007 Evaluating optical aberration using fluorescent microspheres: methods, analysis, and corrective actions *Methods Cell Biol.* **81** 397–413
- [102] Hiraoka Y, Seday J W and Agard D A 1990 Determination of the three-dimensional behaviour in epifluorescence microscopy *Biophys. J.* **57** 325–33
- [103] Cole R W, Jinadasa T and Brown C M 2011 Measuring and interpreting point spread functions to determine confocal microscope resolution and ensure quality control *Nature Protocols* **6** 1929–41
- [104] Moerner W E 2007 New directions in single-molecule imaging and analysis *Proc. Natl Acad. Sci. USA* **104** 12596–602
- [105] Rhodes S K, Barty A, Roberts A and Nugent K A 1990 Sub-wavelength characterisation of optical focal structures *Opt. Commun.* **145** 9–14
- [106] Beverage J L, Shack R V and Descour M R 2002 Measurement of the three-dimensional microscope point spread function using a Shack Hartmann wavefront sensor *J. Microsc.* **205** 61–75
- [107] Lineberg P J 1954 Measurement of contrast transmission characteristics in optical image formation *Opt. Acta* **1** 80–9
- [108] Barakat R and Houston A 1964 Line spread function and cumulative line spread function for systems with rotational symmetry *J. Opt. Soc. Am.* **54** 768–73
- [109] Barakat R and Houston A 1965 Line spread and edge spread functions in the presence of off-axis aberrations *J. Opt. Soc. Am.* **55** 1132–5
- [110] Mallick S 1966 Measurement of optical transfer function with polarization interferometer *Opt. Acta* **13** 247–53
- [111] Birch K G 1961 A scanning instrument for the measurement of optical frequency response *Proc. Phys. Soc.* **27** 901–12
- [112] Waterworth M D 1967 A new method for the measurement of optical transfer functions *J. Sci. Instrum.* **44** 195–9
- [113] Kuttner P 1968 An instrument for determining the transfer function of optical systems *Appl. Opt.* **7** 1029–33
- [114] Tatian B 1965 Method for obtaining the transfer function from the edge response function *J. Opt. Soc. Am.* **55** 1014–9
- [115] Yeaton E C 1969 A comparison of two different methods of OTF measurement *Appl. Opt.* **8** 2541–4
- [116] Takacs P Z, Li M X, Furenlid K and Church E L 1993 Step-height standard for surface profiler calibration *Proc. SPIE* **1995** 235–44
- [117] Mainsah E, Dong W and Stout K J 1996 Problems associated with the calibration of optical probe based topography instruments *Measurement* **17** 173–81
- [118] Hacking K 1958 An optical method of obtaining the frequency response of a lens *Nature* **181** 1158–9
- [119] Pouleau J 1975 Modulation transfer function measurement of optical systems in the visible and infra-red (5 to 20 μm) range *Opt. Acta* **22** 339–46
- [120] Basuray A and Shah M 1991 Optical-transfer-function evaluation utilizing a rotationally symmetric sinusoidal grating and a linear sinusoidal grating of finite height *J. Opt. Soc. Am. A* **8** 212–6
- [121] Novak E, Ai C and Wyant J C 1997 Transfer function characterization of laser Fizeau interferometer for high-spatial-frequency phase measurements *Proc. SPIE* **3134** 114–21
- [122] Boreman G D and Yang S 1995 Modulation transfer function measurement using three- and four-bar targets *Appl. Opt.* **34** 8050–2
- [123] Nijhawan O P, Datta P K and Bhushan J 1975 On the measurement of MTF using periodic patterns of rectangular and triangular wave forms *Nouv. Rev. Opt.* **6** 33–6
- [124] Thurman S T 2011 OTF estimation using a Siemens star target *Imaging Systems and Applications (Toronto)* p IMC5
- [125] Wood M C, Wang X, Zheng B, Li S, Chen W and Liu H 2008 Using contrast transfer function to evaluate the effect of motion blur on microscope image quality *Proc. SPIE* **6857** 68570F
- [126] Kubota H and Ohzu H 1957 Method of measurement of response function by means of random chart *J. Opt. Soc. Am.* **47** 666–7
- [127] Daniels A, Boreman G D, Ducharme A D and Sapir E 1995 Random transparency targets for modulation transfer function measurement in the visible and infrared regions *Opt. Eng.* **34** 860–8
- [128] Levy E, Peles D, Opher-Lipson M and Lipson S G 1999 Modulation transfer function of a lens measured with a random target method *Appl. Opt.* **38** 679–83
- [129] Pieralli C 1994 Estimation of point-spread functions and modulation-transfer functions of optical devices by statistical properties of randomly distributed surfaces *Appl. Opt.* **35** 8186–93
- [130] Wittenstein W, Fontanella J C, Newbery A R and Baars J 1982 The definition of the OTF and the measurement of aliasing for sampled imaging systems *Opt. Acta* **29** 41–50
- [131] Park S K, Schowengerdt R and Kaczynski M-A 1984 Modulation-transfer-function analysis for sampled image systems *Appl. Opt.* **23** 2572–82
- [132] Marchywka M and Socker D G 1992 Modulation transfer function measurement technique for small pixel detectors *Appl. Opt.* **31** 7198–213
- [133] Yashchuk V V, McKinney W R and Takacs P Z 2008 Binary pseudo-random grating standard for calibration of surface profilometers *Opt. Eng.* **47** 073602
- [134] Barber S K, Soldate P, Anderson E D, Cambie R, McKinney W R, Takacs P Z, Voronov D L and Yashchuk V V 2009 Development of pseudo-random binary gratings and arrays for calibration of surface profile metrology tools *J. Vac. Sci. Technol. B* **27** 3213–9
- [135] Barber S K, Soldate P, Anderson E D, Cambie R, Marchesini S, McKinney W R, Takacs P Z, Voronov D L and Yashchuk V V 2009 Binary pseudo-random gratings and arrays for calibration of modulation transfer function of surface profilometers: recent developments *Proc. SPIE* **7448** 744802

- [136] Barber S K, Anderson E, Cambie R, Marchesini S, McKinney W R, Takacs P Z, Voronov D L and Yashchuk V V 2010 Stability of modulation transfer function calibration of surface profilometers using binary pseudo-random gratings and arrays with non-ideal groove shapes *Opt. Eng.* **49** 053606
- [137] Yashchuk V V, McKinney W R and Takacs P Z 2007 Binary pseudo-random grating as a standard test surface for measurement of modulation transfer function of interferometric microscopes *Proc. SPIE* **6704** 670408
- [138] Yashchuk V V, Anderson E H, Barber S K, Bouet N, Cambie R, Conley R, McKinney W R, Takacs P Z and Voronov D L 2011 Calibration of the modulation transfer function of surface profilometers with binary pseudorandom test standards: expanding the application range to Fizeau interferometers and electron microscopes *Opt. Eng.* **50** 093604
- [139] Slyusarev G C 1970 *Sov. J. Opt. Technol.* **37** 299
- [140] Shymga V V 1975 *Sov. J. Opt. Technol.* **41** 81
- [141] Vallmitjana S, Navajas D, Barandalla J J and de F Moneo J R 1983 A simple method of evaluating the polychromatic modulation transfer function for photographic systems *J. Opt.* **14** 25–8
- [142] Juvells I, Vallmitjana S, Ros D and de F Moneo J R 1983 Numerical evaluation of the two-dimensional modulation transfer function by means of spot diagram comparison with experimental measurements *J. Opt.* **14** 293–7
- [143] Schrader M, Kozubek M, Hell S W and Wilson T 1997 Optical transfer functions of 4pi confocal microscopes: theory and experiment *Opt. Lett.* **22** 436–8
- [144] Cotte Y, Toy F M, Arfire C, Kou S S, Boss D, Bergoënd I and Depeursing C 2011 Realistic 3D coherent transfer function inverse filtering of complex fields *Biomed. Opt. Express* **2** 2216–30
- [145] Hopkins H H 1955 Interferometric methods for the study of diffraction images *Opt. Acta* **2** 23–9
- [146] Selligson J L 1981 Phase measurement in the focal region of an aberrated lens *PhD Thesis*
- [147] Dändliker R, Märki I, Salt M and Nesci A 2004 Measuring optical phase singularities at subwavelength resolution *J. Opt. A: Pure Appl. Opt.* **6** S189–96
- [148] Schrader M and Hell S W 1996 Wavefronts in the focus of a light microscope *J. Microsc.* **184** 143–8
- [149] Török P and Kao F-J 2002 Point-spread function reconstruction in high aperture lenses focusing ultra-short laser pulses *Opt. Commun.* **213** 97–102
- [150] Juškaitis R and Wilson T 1998 The measurement of the amplitude point spread function of microscope objective lenses *J. Microsc.* **189** 8–11
- [151] Walford J N, Nugent K A, Roberts A and Scholten R E 2002 High-resolution phase imaging of phase singularities in the focal region of a lens *Opt. Lett.* **27** 345–7
- [152] Marian A, Charrière F, Colomn T, Montfort F, Kühn J, Marquet P and Depeursing C 2006 On the complex three-dimensional amplitude point spread function of lenses and microscope objectives: theoretical aspects, simulations and measurements by digital holography *J. Microsc.* **225** 156–69
- [153] Hanser B M, Gustafsson M G L, Agard D A and Sedat J W 2004 Phase-retrieved pupil functions in wide-field fluorescence microscopy *J. Microsc.* **216** 32–48
- [154] Quiney H M, Williams G J and Nugent K A 2008 Non-iterative solution of the phase retrieval problem using a single diffraction measurement *Opt. Express* **16** 6896–903
- [155] Lee U W and Bond L J 1993 Characterization of ultrasonic imaging systems using transfer functions *Ultrasonics* **31** 405–15
- [156] Oppelt R and Ermert H 1984 Transfer function analysis of a quasioptical ultrasonic imaging system *Ultrason. Imaging* **6** 324–41
- [157] Zinin P, Weise W and Boseck S 1998 Detection of the defocused transfer function of a confocal reflection acoustic microscope (SAM) by imaging of a step and a sphere *Proc. SPIE* **3581** 347–58
- [158] Weise W, Zinin P, Wilson T, Briggs A and Boseck S 1996 Imaging of spheres with the confocal scanning optical microscope *Opt. Lett.* **21** 1800–2
- [159] Zinin P, Weise W, Lobkis O and Boseck S 1998 The theory of three dimensional imaging of strong scatterers in scanning acoustic microscopy *Wave Motion* **25** 213–36
- [160] Zinin P, Weise W, Zhai T, Briggs G A D and Boseck S 1997 Determination of the defocused transfer function of a confocal reflection microscope by imaging of a sphere *Optik* **107** 45–8
- [161] Weise W, Zinin P, Briggs A, Wilson T and Boseck S 1998 Examination of the two dimensional pupil function in coherent scanning microscopes using spherical particles *J. Acoust. Soc. Am.* **104** 181–91
- [162] Wolfe C R, Downie J D and Lawson J K 1996 Measuring the spatial frequency transfer function of phase-measuring interferometers for laser optics *Proc. SPIE* **2870** 553–7
- [163] Baker L R 1989 An interferometer for measuring the spatial frequency response to a lens system *Proc. Phys. Soc. B* **68** 871–80
- [164] Hariharan P and Sen D 1960 A simple interferometric arrangement for the measurement of optical frequency response characteristics *Proc. Phys. Soc. Lond.* **75** 434–8
- [165] Kelsall D 1959 *Proc. Phys. Soc. Lond.* **73** 465
- [166] Montgomery A J 1966 Two methods of measuring optical transfer functions with an interferometer *J. Opt. Soc. Am.* **54** 624–8
- [167] Tsuruta T 1963 Measurement of transfer functions of photographic objectives by means of a polarizing shearing interferometer *J. Opt. Soc. Am.* **53** 1156–60
- [168] Kelsall D 1973 Rapid interferometric technique for MTF measurements in the visible or infrared region *Appl. Opt.* **12** 1398–9
- [169] Mercer C R and Creath K 1994 Liquid-crystal point-diffraction interferometer *Opt. Lett.* **19** 916–8
- [170] Griffin D W 2001 Phase-shifting shearing interferometer *Opt. Lett.* **26** 140–1
- [171] Wyant J C 1976 A simple interferometric MTF instrument *Opt. Commun.* **19** 120–1
- [172] Wyant J C 1975 OTF measurements with a white light source: an interferometric technique *Appl. Opt.* **14** 1613–5
- [173] Arecchi F T, Bassan M, Jacobs S F and Molesini G 1979 MTF measurement via diffraction shearing with optically superimposed gratings *Appl. Opt.* **18** 1247–8
- [174] Grover C P and van Driel H M 1980 Autocorrelation method for measuring the transfer function of optical systems *Appl. Opt.* **19** 900–4
- [175] Indebetouw G 1983 Some experiments in partially coherent imaging and modulation transfer function evaluation *Appl. Phys. B* **32** 21–4
- [176] Sheppard C J R 1986 The spatial frequency cut-off in three dimensional imaging *Optik* **72** 131–3
- [177] Sheppard C J R 1986 The spatial frequency cut-off in three dimensional imaging ii *Optik* **74** 128–9
- [178] Mandal R, Palodhi K, Coupland J, Leach R K and Mansfield D 2011 Measurement of the point spread function in coherence scanning interferometry *ICoNTOPII: Proc. Int. Conf. on Trends in Optics and Photonics* pp 252–7

- [179] Palodhi K, Coupland J and Leach R K 2011 Measurement of the point spread function in coherence scanning interferometry *Proc. Int. Conf. on Metrology Properties of Engineering Surfaces* 119–203
- [180] Woolliams P D, Ferguson R A, Hart C, Grimwood A and Tomlins P H 2010 Spatially deconvolved optical coherence tomography *Appl. Opt.* **41** 2014–21
- [181] Woolliams P D and Tomlins P H 2011 Estimating the resolution of a commercial optical coherence tomography system with limited spatial sampling *Meas. Sci. Technol.* **22** 065502
- [182] Chu J, Wang Q, Lehan J P, Gao G and Griesmann U 2008 Measuring the phase transfer function of a phase shifting interferometer *Proc. SPIE* **7064** 70640C